AFRL-AFOSR-VA-TR-2016-0343

BIOMOLECULAR PROGRAMMING OF DISCRETE NANOMATERIALS FOR SENSORS, TEMPLATES AND MIMICS OF NATURAL NANOSCALE ASSEMBLIES

Nathan Gianneschi
UNIVERSITY OF CALIFORNIA SAN DIEGO

10/17/2016
Final Report

Air Force Research Laboratory
AF Office Of Scientific Research (AFOSR)/ RTB2
Arlington, Virginia 22203
Air Force Materiel Command

REPORT DOCUMENTATION PAGE

Form Approved
OMB No. 0704-0188

1. REPORT DATE *(DD-MM-YYYY)*	2. REPORT TYPE	3. DATES COVERED *(From - To)*
08-11-2016	Final Performance	01 Jun 2011 to 31 May 2016

4. TITLE AND SUBTITLE
BIOMOLECULAR PROGRAMMING OF DISCRETE NANOMATERIALS FOR SENSORS, TEMPLATES AND MIMICS OF NATURAL NANOSCALE ASSEMBLIES

5a. CONTRACT NUMBER

5b. GRANT NUMBER
FA9550-11-1-0105

5c. PROGRAM ELEMENT NUMBER
61102F

6. AUTHOR(S)
Nathan Gianneschi

5d. PROJECT NUMBER

5e. TASK NUMBER

5f. WORK UNIT NUMBER

7. PERFORMING ORGANIZATION NAME(S) AND ADDRESS(ES)
UNIVERSITY OF CALIFORNIA SAN DIEGO
9500 GILMAN DR DEPT 621, OFFICE OF CONTRACT & GRANT ADMIN. 09
LA JOLLA, CA 92093-0621 US

8. PERFORMING ORGANIZATION REPORT NUMBER

9. SPONSORING/MONITORING AGENCY NAME(S) AND ADDRESS(ES)
AF Office of Scientific Research
875 N. Randolph St. Room 3112
Arlington, VA 22203

10. SPONSOR/MONITOR'S ACRONYM(S)
AFRL/AFOSR RTB2

11. SPONSOR/MONITOR'S REPORT NUMBER(S)
AFRL-AFOSR-VA-TR-2016-0343

12. DISTRIBUTION/AVAILABILITY STATEMENT
A DISTRIBUTION UNLIMITED: PB Public Release

13. SUPPLEMENTARY NOTES

14. ABSTRACT
We have worked on the development of biomolecule-polymer conjugates as responsive elements for assembly of complex morphology switchable nanomaterials, and have combined this with an effort in nature-inspired materials with a particular focus on synthetic, or artificial polymeric organelles, including melanosomes. Relevance of these projects to the DOD interests include the possibility of employing the resulting materials in advanced biochemical sensors, where recognition elements combined with stability and long term use are needed; hence our interest in stabilized but responsive biomolecular materials and conjugates between 2011 and 2016. In terms of melanin work, we see strong relevance in these bioinspired materials that are capable of acting as structural color elements, with unusually high refractive indices and with an understanding of synthetic processes leading to morphological control. This would lead to an ability to develop materials that have iridescent structural color, but capable of broad band absorbance, combined with unusual magnetic properties. The fact that very little is known about their natural biosynthesis, and their properties in general, means there is a rich source of chemical information to mine, and potentially utilize in new device applications. Thirdly, we have developed liquid cell TEM (LCTEM) as a means for studying these complex responsive systems.

15. SUBJECT TERMS
nanomaterials, sensors, templates

16. SECURITY CLASSIFICATION OF:

a. REPORT	b. ABSTRACT	c. THIS PAGE	17. LIMITATION OF ABSTRACT	18. NUMBER OF PAGES	19a. NAME OF RESPONSIBLE PERSON
Unclassified	Unclassified	Unclassified	UU		DELONG, HUGH
					19b. TELEPHONE NUMBER *(Include area code)* 703-696-7722

Grants Agreement Award#: FA9550-11-1-0105

FINAL PERFORMANCE REPORT

BIOMOLECULAR PROGRAMMING OF DISCRETE NANOMATERIALS FOR SENSORS, TEMPLATES AND MIMICS OF NATURAL NANOSCALE ASSEMBLIES

Report for the period: 6/1/2011-8/31/2016

Submitted to
Air Force Office of Scientific Research

By
The University of California, San Diego

Principle Investigator:
Nathan C. Gianneschi, Dept. Chemistry & Biochemistry, University of California, San Diego
Tel: (858)-373-7448 e-mail: ngianneschi@ucsd.edu

Research Topic Chief:
Dr. Hugh C. DeLong, Program Manager for Natural Materials and Systems,
AFOSR/RSL, (703) 696-7722, hugh.delong@afosr.af.mil

October 8th, 2016

(PECASE) Biomolecular Programming of Discrete Nanomaterials for Sensors, Templates and Mimics of Natural Nanoscale Assemblies

Abstract

Over the past five years, we have endeavored to develop biomolecule-polymer conjugates as responsive elements for assembly of complex morphology switchable nanomaterials, and have combined this with an effort in nature-inspired materials with a particular focus on synthetic, or artificial polymeric organelles, including melanosomes. As part of these studies into complex materials, we have developed a robust and pioneering program in the development of liquid cell TEM (LCTEM), and more recently in variable temperature LCTEM (VT-LCTEM) methodologies for looking at porous materials including organic systems and coordination networks. In this report we will summarize our efforts in these areas over the duration of the program.

Objectives

Objective 1: To develop biomolecule programming of discrete, soft polymeric materials. These studies can be divided into several parts: 1) Exploration of chemical parameter space to determine limits of the approach utilizing DNA, peptide, and enzyme driven morphological transitions. 2) Development of protein-amphiphiles for spatially organized multi-protein assemblies as semi-synthetic mimics of viral capsid formation. 3) Optimization and development of a novel inorganic nanostructure templation strategy. 4) Development of electron microscopy methods coupled with theoretical investigations to enable characterization and predictive analysis.

Objective 2: To explore morphology switchable materials in biochemical systems. The ability to utilize morphology switches in detection of biochemical events will be a special focus of this work and will involve a study of various interactions with living systems. FRET-based systems will be utilized for detecting morphology change and/or enzyme-triggering. Motivation for exploring the fundamental aspects and basic limitations of these materials in a variety of environments comes from the possibility for developing *in vivo* sensors and stimuli-responsive systems for detection and response.

Results (2011-2016)

SUMMARY

This report will be broken into sections describing work supported by this PECASE award. These include a review of our work on biomolecule programmed polymeric nanomaterials. In addition, we will describe our pioneering efforts to develop Liquid Cell TEM methodologies (LCTEM). Finally, we will describe our work on the development of melanin-based materials. Overall, we have addressed our two main objectives in terms of an exploration of biomolecule programming of soft matter, and have extended this to non-informational biopolymers with an effort in the space of melanin-like artificial nanostructures and structural and functional mimics of natural melanin. The report will summarize previously published works in the context of the PECASE award, and will give a more detailed description of work pending publication that has and will extend beyond the end date of the award.

(PECASE) Biomolecular Programming of Discrete Nanomaterials for Sensors, Templates and Mimics of

SECTION 1: *Biomolecule Programmed Polymers and Polymeric Nanostructures*

Introduction

Our original proposal was predicated on the idea that soft, discrete nanomaterials are difficult to control in terms of both their primary structures, and their ability to undergo phase transitions by design following their initial formation. Therefore, assembly processes and transformations that could be actuated by specific, informational stimuli became a very specific focus of our work since 2011 on this AFOSR funded PECASE award program. Indeed, from this starting point came our efforts to develop both new characterization tools (**Section 2** of this report on LCTEM), and our pushing towards new ways of utilizing non-informational, but highly abundant biomolecules including melanins, or polydopamines (**Section 3** of this report on artificial melanin nanostructures).

Summary of Translational Outcomes

We have had success in our efforts to develop both peptide and nucleic acid polymer conjugates that are capable of assembly into three-dimensional, switchable, discrete soft nanomaterials. These materials have been translated into a variety of other applications including as addressable handles for switchable liquid crystalline sensors (Ma, C. D.; Adamiak, L.; Miller, D. S.; Wang, X.; Gianneschi, N. C.; Abbott, N. L. "Liquid Crystal Interfaces Programmed with Enzyme-Responsive Polymers and Surfactants" *Small* **2015**, 11, 5747-5751.), which is work we have conducted in collaboration with Prof. Nick Abbott's group at U. of Wisconsin. In addition, we have utilized this new class of materials in tissue targeted delivery of drugs and diagnostic agents to diseased tissue in heart disease and cancer applications (Callmann, C. E.; Barback, C. V.; Thompson, M. P.; Hall, D. J.; Mattrey, R. F.; Gianneschi, N. C. "Therapeutic Enzyme-Responsive Nanoparticles for Targeted Delivery and Accumulation in Tumors" *Adv. Mat.* **2015**, *27*, 4611-4615. Nguyen, M. M.; Carlini, A. S.; Chien, M. –P.; Sonnenberg, S.; Luo, C.; Braden, R. L.; Osborn, K. G.; Li, Y.; Gianneschi, N. C.; Christman, K. L. "Enzyme-Responsive Nanoparticles for Targeted Accumulation and Prolonged Scaffold Retention in Heart Tissue After Myocardial Infarction" *Advanced Materials* **2015**, 27, 5547-5552.); this is work that has been funded by NIH, relates to disease associate applications, but was fully enabled by the basic materials science funded by the AFOSR PECASE program.

Summary of Impact and Importance of Work Related to Biopolymer Programmed Systems

Development of nucleic acid programmed amphiphilic polymers as tunable, responsive materials:
These materials have been studied from a fundamental standpoint, wherein they undergo switchable morphology in response to specific interactions with complementary DNA and RNA strands. This has lead to the discovery that these materials are exceptionally resistant to nuclease degradation and can be used as highly efficient delivery systems enabling intracellular delivery of oligonucleotides having efficacy in gene regulation. These materials are currently under investigation in a range of settings, where transport of oligonucleotides into cells and tissues are of interest.
Related Publications:

(PECASE) Biomolecular Programming of Discrete Nanomaterials for Sensors, Templates and Mimics of

a. Chien, M. –P.; Rush, A. M.; Thompson, M. P.; **Gianneschi, N. C.** “Progammable Shape-Shifting Micelles” *Angew. Chem. Int. Ed.* **2010**, *49*, 5076-5080. PMID: 20533475 **(105 citations)**
b. Chien, M. –P.; Thompson, M. P.; **Gianneschi, N. C.** “Smart Lipids for Programmable Nanomaterials” *Nano Letters* **2010**, *10*, 2690-2683. **(40 citations)**
c. Rush, A. M.; Thompson, M. P.; Tatro, E. T.; Gianneschi, N. C. “Nuclease-resistant DNA via High Density Packing in Polymeric Micellar Nanoparticle Coronas” *ACS Nano* **2013**, *7*, 1379-1387. PMCID: PMC3608424 **(25 citations)**
d. James, C. R.; Rush, A. M.; Insley, T.; Vukovic, L.; Kral, P.; **Gianneschi, N. C.** “Poly(oligonucleotide)” *J. Am. Chem. Soc.* **2014**, *136*, 11216-11219. PMID: 25077676; PMCID: PMC4140503.
e. Rush, A. M.; Nelles, D. A.; Blum, A. P.; Barnhill, S. A.; Tatro, E. T.; Yeo, G. W.; **Gianneschi, N. C.** “Intracellular mRNA Regulation with Self-Assembled Locked Nucleic Acid Polymer Nanoparticles” *J. Am. Chem. Soc.* **2014**, *136*, 7615-7618. PMID: 24827740; PMCID: PMC4046771 **(17 citations)**

Development and invention of dense, peptide brush polymers and copolymers prepared via graft-through polymerization to generate highly proteolytically stable peptides for biological and biomedical applications.

This work has involved a concerted effort to develop basic polymer chemistry to prepare unusually densely packed peptides as brush polymers. The resulting materials are of interest as packaging systems for the delivery of highly proteolytically stable peptides capable of entering cells, and escaping endosomes to have action in the cytosol. Moreover, the approach overcomes significant barriers that have traditionally prevented very promising peptides from being useful in clinical settings.
Related Publications:

a. Hahn, M. E.; Randolph, L. M.; Adamiak, L.; Thompson, M. P.; **Gianneschi, N. C.** “Polymerization of a Peptide-Based Enzyme Substrate” *Chem. Commun.* **2013**, *49*, 2873-2875. PMCID: PMC3608426 **(18 citations)**
b. Kammeyer, J. K.; Blum, A. P.; Adamiak, L. Hahn, M. E.; **Gianneschi, N. C.** “Polymerization of Protecting-Group-Free Peptides via ROMP” *Polymer Chemistry* **2013**, *4*, 3929-3933. PMID: 24015154; PMCID: PMC3762507. **(17 citations)**
c. Thompson, M.P.; Randolph, L.M;, James, C.R;, Davalos, A.N;, Hahn, M.E;, **Gianneschi, N.C.** “Labelling Polymers and Micellar Nanoparticles via Initiation, Propagation and Termination with ROMP.” *Polymer Chem*. **2014**, *5*, 1954-1964. PubMed PMID: 24855496; PMCID: PMC4023353.
d. Blum, A. P.; Kammeyer, J. K.; Yin, J.; Crystal, D. T.; Rush, A. M.; Gilson, M. K. **Gianneschi, N. C.** “Peptides Displayed as High Density Brush Polymers Resist Proteolysis and Retain Bioactivity” *J Am. Chem. Soc.* **2014**, *136*, 15422-15437. PMID: 25314576; PMCID: PMC4227725 **(13 citations)**

Invention of enzyme-directed assembly of nanoparticle probes for targeted accumulation in tumors and in heart tissue post-heart attack:

We have shown that materials, responsive to proteolytic enzymes (matrix metalloproteinases) associated with metastatic tumor tissue and with damaged heart tissue following myocardial infarction, will accumulate and be retained within these tissues following intravenous injection. This approach represents a significant departure from other targeting methods that make use of passive accumulation based on the size of the nanoparticle, or through active binding to receptors based on dissociation constants associated with specific ligand-receptor pairs. Our approach involves

enzymatic reactions that physically trap polymeric nanomaterials within the tissue, preventing the materials from leaking back into the vasculature once they exit the blood vessels. The particles are designed to be small (10-20 nm) in diameter, but then enlarge to many microns in size within the tissue. This means that we rely on enzymatic activity to kinetically trap materials in place. This has lead to our ability to collect fluorescently labeled materials within tumors and to deliver drugs, having a beneficial labeling and/or therapeutic effect respectively. This effort has involved the development of entirely new materials on the benchtop, through to testing in live animal models for cancer and heart attack. The work consists of a set of interconnected projects involving many student and postdoctoral researchers linking advanced materials development to translational nanomedicine.
Related Publications:

a. Ku, T.-H.; Chien, M.-P.; Thompson, M. P.; Sinkovits, R. S.; Olson, N. H; Baker, T. S.; **Gianneschi, N. C.** "Controlling and Switching the Morphology of Micellar Nanoparticles with Enzymes" *J. Am. Chem. Soc.* **2011**, *133*, 8392-8395. PMID: 21462979; PMCID: PMC3756928 **(84 citations)**
b. Chien, M. –P.; Thompson, M. P.; Lin, E. C.; **Gianneschi, N. C.** "Fluorogenic Enzyme-Responsive Micellar Nanoparticles" *Chemical Science* **2012**, *3*, 2690-2694. PMCID: PMC3622269 **(22 citations)**
c. Randolph, L. M.; Chien, M. –P.; **Gianneschi, N. C.** "Biological Stimuli and Biomolecules in the Assembly and Manipulation of Nanoscale Polymeric Particles" *Chem. Sci.* **2012**, *3*, 1363-1380 **(54 citations)**
d. Chien, M. –P.; Thompson, M. P.; Barback, C. V.; Hall, D. J.; **Gianneschi, N. C.** "Enzyme-Directed Assembly of a Nanoparticle Probe in Tumor Tissue" *Advanced Materials.* **2013**, *25*, 3599-3604. PMID: 23712821; PMCID: PMC4108424. **(34 citations)**
e. Chien, M.-P.; Carlini, A. S.; Hu, D.; Barback, C. V.; Rush, A. M.; Hall, D. J.; Orr, G.; **Gianneschi, N. C.** "Enzyme-Directed Assembly of Nanoparticles in Tumors Monitored by In Vivo Whole Animal and Ex Vivo Super Resolution Fluorescence Imaging" *J. Am. Chem. Soc.* **2013**, *135,* 18710-18713. PMID: 24308273; PMCID: PMC4021865. **(36 citations)**
f. Callmann, C. E.; Barback, C. V.; Thompson, M. P.; Hall, D. J.; Mattrey, R. F.; **Gianneschi, N. C.** "Therapeutic Enzyme-Responsive Nanoparticles for Targeted Delivery and Accumulation in Tumors" *Adv. Mat.* **2015**, *27*, 4611-4615. **(26 citations)**
g. Blum, A. P.; Kammeyer, J. K.; Rush, A. M.; Callmann, C. E.; Hahn, M. E. **Gianneschi, N. C.** "Stimuli-Responsive Nanomaterials for Biomedical Applications" *J. Am. Chem. Soc.* **2015**, *137,* 2140-2154. **(71 citations)**

Summary of Recent Publications and their Impact from the Final Year (2015-2016)

1) Ma, C. D.; Adamiak, L.; Miller, D. S.; Wang, X.; Gianneschi, N. C.; Abbott, N. L. "Liquid Crystal Interfaces Programmed with Enzyme-Responsive Polymers and Surfactants" *Small* **2015**, 11, 5747-5751

Biologically active peptide–polymer amphiphiles (PPAs) were synthesized and assembled at the interfaces of liquid crystal (LC) microdroplets, to prove the strategy of triggering the ordering transitions in LC microdroplets in response to targeted biomolecular events.

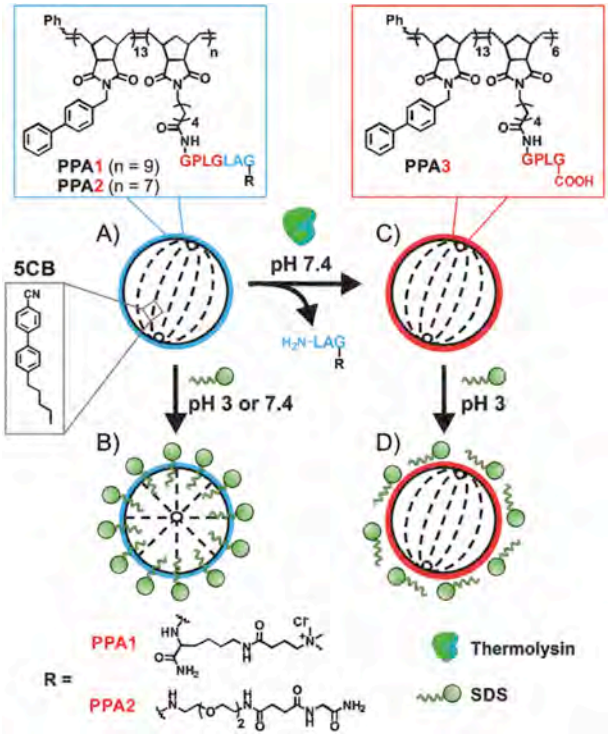

Figure 1. Schematic diagram for response of PPA-programmed LC microdroplets to

PPAs were incorporated with biphenyl side chains that promote interfacial assembly of the PPAs and peptide side chains that can be enzymatically processed. We found that the PPAs form stable Langmuir films at the surface of water and that differences in the molecular structure of the PPAs are clearly reflected in the surface pressure-area isotherms. Specifically, we observed that the PPA synthesized to represent the product of an enzymatic reaction exhibits sensitivity to pH consistent with the presence of a free carboxylic acid group. These pH-induced changes in interfacial properties were also evident at aqueous–LC interfaces, and resulted in reordering of the LCs based on the differential interactions of an ionic surfactant with the reactant and product of the enzymatic reaction. When combined, these results guided us to experimental conditions that permitted the use of PPAs to report on enzymatic processing of oligopeptide substrates at the interfaces of LC droplets. We show that simple surfactants can differentially interact with the PPA before and after enzymatic processing to enable striking and easily transduced changes in the ordering of an LC. Furthermore, we performed proof-of-concept studies of the enzymatic processing of PPA-decorated LC droplets using this strategy. An additional important conclusion of our study is that simple surfactants offer the basis of a general and facile strategy potentially applicable to a wide range of responsive macromolecular species that assemble at LC interfaces.

<u>Structural and functional study of polymer/LC interactions</u>

To answer questions related to the structure and architecture of the amphiphilic polymers and their interactions with liquid crystals, we synthesized a library of ROMP-based polymers with different hydrophobic side chains in order to develop rational design principles for amphiphilic polymers that can trigger responses in liquid crystals.

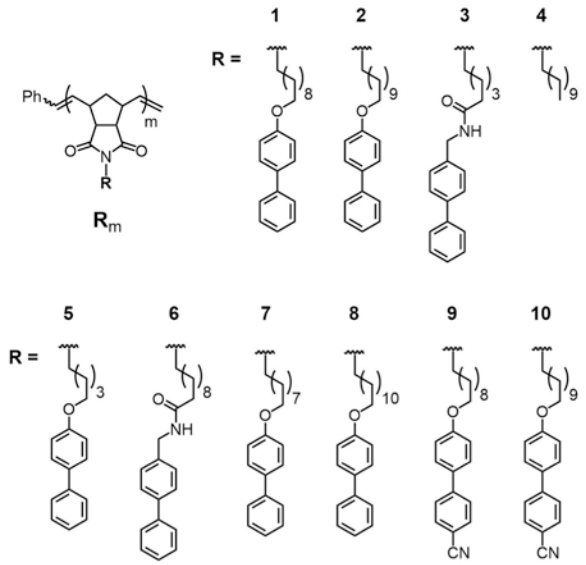

Figure 2. The chemical structures for the homopolymers with hydrophobic side-chains

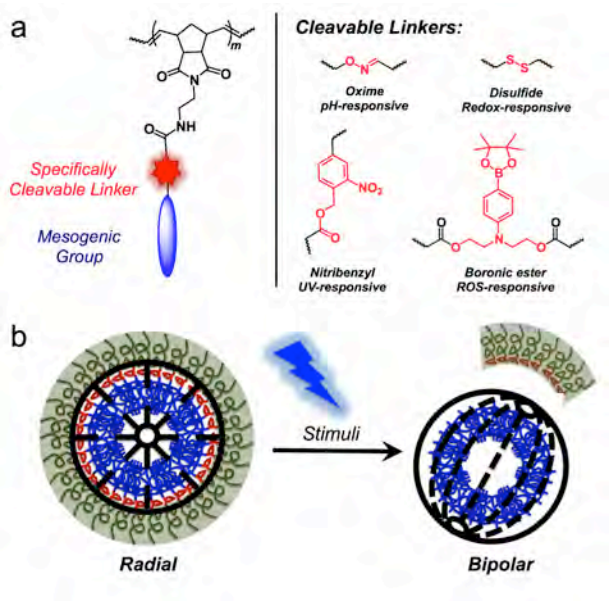

Figure 3. a) General designs of stimuli-responsive ROMP polymer with 4 types of cleavable linkers; b) Schematic diagram for stimuli-responsive ROMP polymer modulating liquid crystal droplets configurations.

First, we studied the effect of the hydrophobic side-group structure on the homeotropic anchoring at the LC/ aqueous interface utilizing homopolymers, including the influence of the hydrocarbon linker length (as **P1, P2, P5, P7, P10**) between polymeric backbone and 5CB-mimic biphenyl functional group, the influence of the linker (such as ester linker in **P5** to amide linker in **P3**, as ester linker in **P1** to amide linker in **P6**), and the influence of functional groups (such as biphenyl group in **P1**, hydrocarbon chain in **P4** and cyano-biphenyl group in **P9**).

Second, to test how the composition and architecture of a polymer can affect the LC/polymer interactions, we investigated the block copolymers and random copolymers with dodecaethylene glycol (PEG-12) as hydrophilic chain. We varied the composition of the block copolymer, and found that the di-block copolymer did not generate as a substantial population of radial liquid crystal droplet configurations. However, the random copolymer architecture can generate radial droplets, and the higher ratio of hydrophobic composition is able to generate more radial configuration droplets.

<u>Building up a versatile and flexible stimuli-responsive ROMP polymeric system for modulating liquid crystal droplets configurations</u>

Liquid crystals confined within micrometer-scale domains have been explored as the basis of a wide range of field- and stimuli-responsive materials for use in technologies spanning from biological sensors to electro-optical devices. Considering to the diversity of ROMP-based polymeric system, we incorporated different types of cleavable linkers into this system to endow versatile stimuli-responsiveness, including oxime linker for pH-responsiveness, disulfide linker

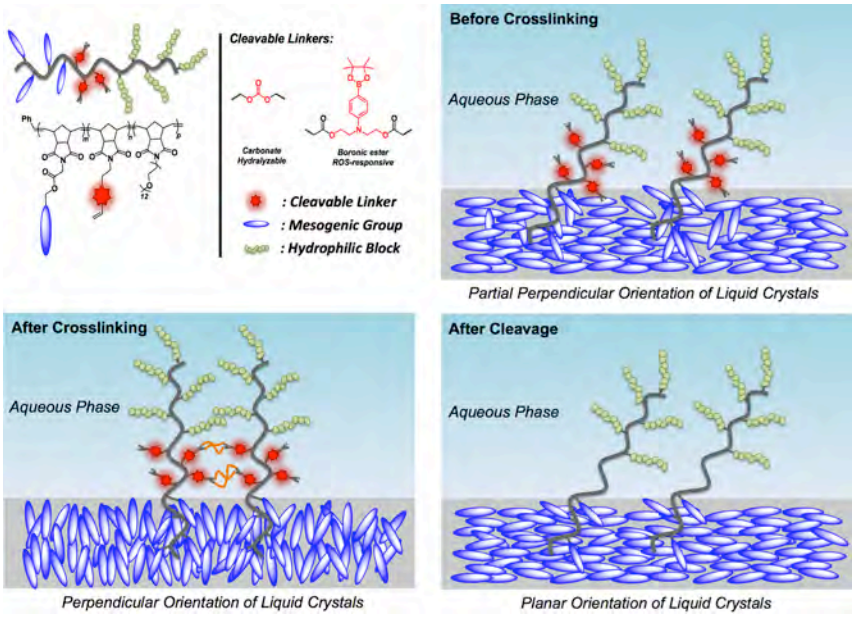

Figure 4. Schematic diagram for using crosslinkable ROMP-based polymers to modulate liquid crystals orientations.

for redox-responsiveness, nitrobenzyl linker for UV-responsiveness and boronic ester linker for ROS-responsiveness. We proved that those cleavable linker-contained homopolymers were able to emulsify with liquid crystal droplets and generate radial configuration. Meantime, by introducing specific stimuli, the linker will be cleaved and the homopolymer will be disassembled from the surface, then the configurations of liquid crystal droplets will change into bipolar. We found that the cleavage of oxime bond did not happen because the diffusion of hydrion cannot reach to pH2 so that the liquid crystal droplets did not show configuration change. However, disulfide bond, and nitrobenzyl bond can be cleaved in a very short time by introducing DTT and UV respectively, resulting in dramatically changes into bipolar configurations. This work will provide fundamental information for designing a stimuli-responsive ROMP-based polymeric system, and it is promising to utilize this system as biosensor to detect some specific behaviors.

Stimuli-responsive crosslinkable ROMP copolymer for liquid crystals modulation

Inspired by the problem that block copolymers cannot generate radial liquid crystal droplets as well as random copolymers, we designed a crosslinkable triblock copolymer, which contains a block with mesogenic group to serve as surfactant, a block which can be crosslinked under UV irradiation and also can be cleaved under certain conditions, and a block to provide hydrophilicity. In these studies, we found that liquid crystal droplets still show bipolar configurations however, they changed to radial after UV-induced crosslinking. It is possible that crosslinking encourages polymers to reside at the surface of liquid crystal droplets allowing them to affect the orientation of the liquid crystals. Moreover, after introducing specific stimuli, the crosslinked network was cleaved and the liquid crystal droplets changed back to bipolar configurations.

Together these initial results suggest we will be capable of developing polymer systems designed around set rules. This will lead to our ability to translate specific chemical interactions and reactions through to large scale changes in liquid crystal structure, and ultimately display properties.

2) Blum, A. P.; Kammeyer, J. K.; Gianneschi, N. C. “Activating Peptides for Cellular Uptake via Polymerization into High Density Brushes” *Chemical Science* **2016**, *7*, 989-994

As with our studies describe in the liquid crystal section above, our group has remained interested in the special functions of peptide-based brush polymer bioconjugates. In this work, we have looked at peptides as synthetic elements in sensors, or in materials in general that traditionally suffer from problems associated with their instability in complex environments. In addition, peptides are degraded by enzymatic processes when used in conjunction or in competition with living systems. We are generally interested in methods for stabilizing biomolecules for use in materials applications, and have pursued this with respect to both peptides and nucleic acids. In this work, we described a simple and potentially widely applicable solution involving the polymerization of a minimally modified amino acid sequence, or short oligopeptide, into a high density brush polymer. Specifically, non-cell penetrating peptides can be rendered competent for cell entry by first including a single Arg or Lys in

their amino acid sequence, if one is not already present, along with a norbornenyl unit. This modified monomer is then subsequently polymerized by ring opening metathesis polymerization (ROMP). We anticipate that this methodology will find broad use in medicine and in materials science, where peptide stability inhibits translation in a variety of applications including responsive materials, sensors and in active surfaces.

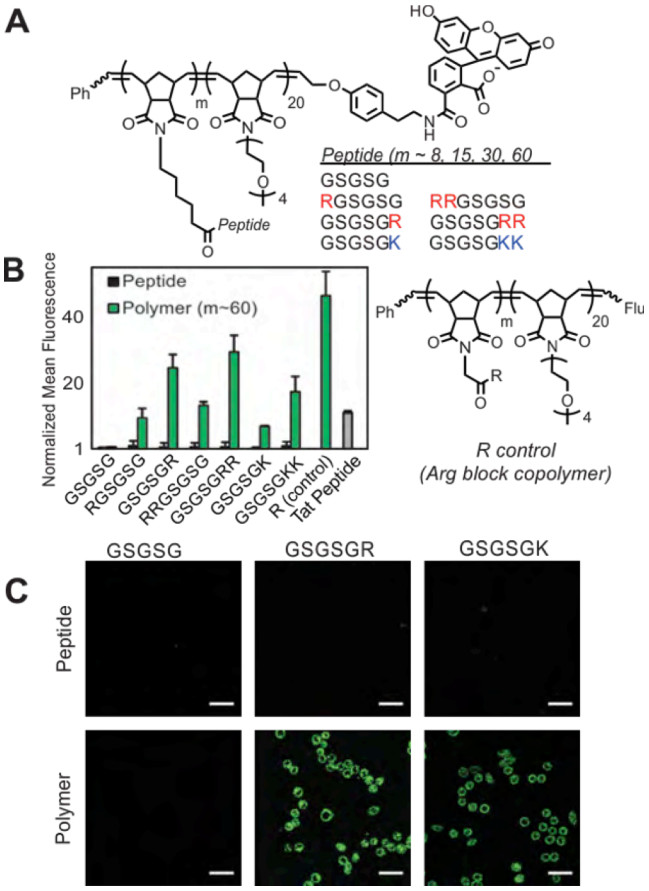

Figure 4. Cellular internalization of GSGSG polymers and analogues. A) Chemical structure of peptide polymers. B) Flow cytometry data showing fluorescent signatures of HeLa cells treated with the peptide polymers (m ~ 60) and their monomeric counterparts. All data are normalized to the vehicle (DPBS) control, which is assigned a value of 1. The R control is a block copolymer that contains a single Arg residue attached via a short linker at each polymer side chain of the first block (m ~ 60). “Flu” is the fluorescein end-label shown in A. C) Live-cell confocal microscopy images showing the average intensities from six consecutive 1 µm slices of HeLa cells treated with peptides and polymers (m ~ 60). Scale bars are 50 µm. In each study, the concentration of material is 2.5 µM with respect to fluorophore.

The chemical diversity inherent to natural and unnatural amino acids enables the formulation of peptides that are selectively and precisely coded for interaction with target receptors and other biological surfaces. This ability has fostered the development and identification of unique natural, semi-synthetic and synthetic peptide sequences capable of diverse medicinal[3-6] and diagnostic[7] applications. We had previously reported a strategy for protecting peptides from proteolysis in which peptides are packaged as high density brush polymers via graft-through ring opening metathesis polymerization (ROMP) of peptide-based monomers, generating structures that are resistant to proteolytic degradation.[8] This strategy does not require chemical modification of the primary amino acid sequence and is, therefore, a facile approach to access formulations of protease-resistant peptides that maintain their inherent function. In this follow on work we found that, when polymerized into a high density brush polymer, peptides bearing a single Arg or Lys can efficienty penetrate cells. Moreover, we propose this as a general strategy for rendering peptides competent for cellular uptake.

To test our strategy, we synthesized a peptide sequence, GSGSG, that does not penetrate cells[8] and appended one or two Arg residues to the N or C terminus, reasoning that these locations would yield the highest likelihood of maintaining the inherent bioactivity of an otherwise intact peptide sequence (Figure 4). These peptides were prepared as fluorescein-labeled[9] peptide controls and also as fluorescein-terminated

brush polymers via the graft-through ROMP strategy[10] (Figure 4A). To ensure solubility of all analogues, the polymers were prepared as block copolymers with a second block containing an OEG (oligoethylene glycol) unit (degree of polymerization (DP) approx. 20), which does not penetrate cells alone.[8] We then quantified the relative extent of uptake of each material in HeLa cells by flow cytometry (Figure 4B). In all cases, the monomeric peptide controls showed fluorescence signals that were indistinguishable from that of the vehicle control. However, peptides containing at least one Arg polymerized with a DP (or "m" in Figure 4) of approximtely 60, were able to penetrate cells as efficiently as a canonical CPP (Tat) at equivalent concentrations of fluorophore. In general, Arg residues appended to the C-terminus (GSGSGR or GSGSGRR) exhibited better intracellular penetration than N-terminal derivatives (RGSGSG or RRGSGSG). This is likely because the N-terminal residues are closer to the polymer backbone and are therefore less likely to engage in interactions with cellular membranes compared to the C-terminal modified analogues. Peptides containing two Arg residues gave more robust fluorescent signals when polymerized than those containing only one in the same position. Interestingly, in all cases, the Arg-containing peptide polymers gave slightly lower values than that of a polymer prepared by polymerizing a single Arg reside (R control polymer – Figure 4B), which we consider to be the maximum theoretical signal that can result from a polymer containing one Arg per polymer side chain. In addition, peptides containing one or two lysine residues were taken up by cells when prepared as polymers (but not as peptides), indicating that the presence of primary amino or guandinium units were sufficient for uptake (Figure 4B). Moreover, the extent of uptake of each polymer was shown to be dependent upon both the degree of polymerization (Figure 5A) and the concentration of material (Figure 5B), suggesting that uptake of these peptides can be improved by increasing either factor.

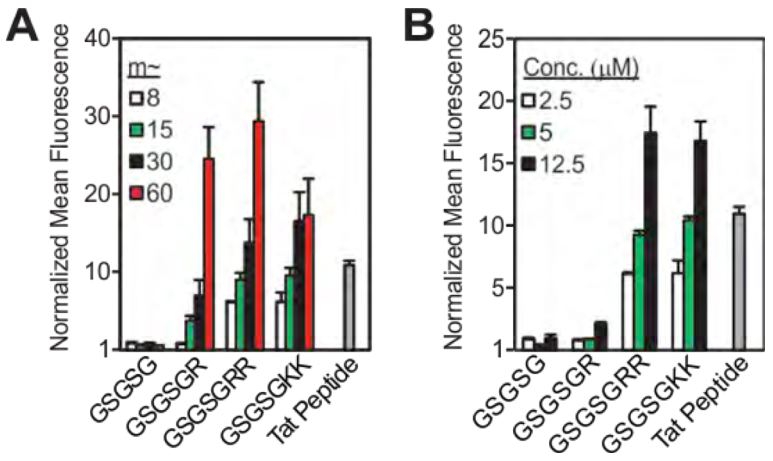

Figure 5. Strategies for increasing cellular uptake of GSGSG anaolgues. Flow cytometry data exploring the impact of (A) degree of polymerization with each polymer at a concentration of 2.5 μM and (B) the concentration of m ~ 8 polymers. All data are normalized to DPBS at a value of 1.

To further verify internalization, treated cells were analyzed by live-cell confocal microscopy via Z-stack analysis (Figure 4C). A fluorescence signal is observed across each 1 μm Z-slice for polymers (m ~ 60) containing Arg or Lys, suggesting the materials are internalized and not simply bound to the surface of the membrane, while no signal is seen for any peptide or the GSGSG parent polymer. Moreover, a mixture of diffuse and punctate fluorescence was observed for Arg/Lys polymers, suggesting cytosolic and compartmental localization of the internalized materials, respectively.

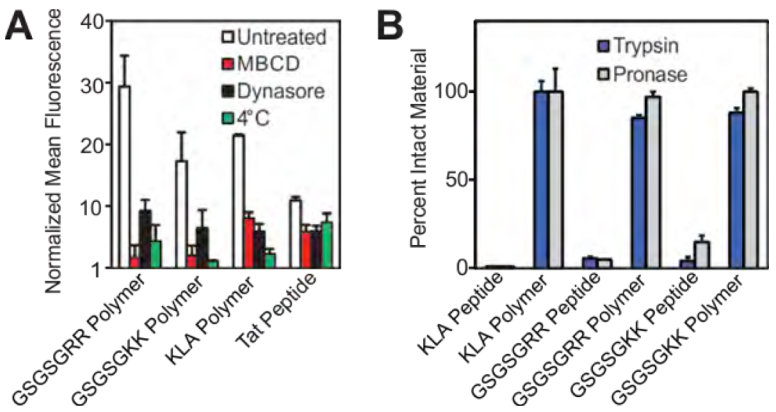

Figure 6. Mechanistic studies and resistance to proteolytic digestion. A) Flow cytometry experiments describing pharmacological inhibition of dynamin-mediated endocytosis by dynasore[(1)] (80 μM), membrane fluidity by methyl-β-cyclodextrin[(2)] (M-βCD, 9.5 mM) or membrane trafficking by a reduction in incubation temperature. Data is normalized to DPBS at a value of 1. B) Proteolytic suscpeptibility was determined by comparing RP-HPLC chromatograms of the material (50 μM) before and after treatment with trypsin or the protease cocktail Pronase (each at 1 μM) for 3 hrs in DPBS.

Having demonstrated successful cellular penetration of our materials, we next assessed the route of cellular entry by employing thermal and pharmacological inhibitors of known uptake pathaways (Figure 6). In all cases, the uptake of the materials are similarly affected by the inhibitors tested, suggesting that each polymer enters the cell by way of endocytosis or another mechanism of membrane disruption in a manner similar to Tat (Figure 6A).

Finally, we confirmed that these materials are resistant to proteolytic degradation. Analysis of reverse-phase HPLC (RP-HPLC) chromatograms before and after proteolytic digestion indicate that, as with our previous studies,[(8)] while the peptide controls are completely degraded into fragments, the peptide polymers show little or no indication of proteolysis after incubation with multiple proteases (Figure 6B).

In summary, we have developed and proven a simple, effective and broadly applicable alternative to existing strategies that enable cell penetration of peptides and most importantly render them resistant to degradation. We have shown this here in the context of in vitro cell uptake and resistance, but these materials will have broader applications in materials science, and in the development of peptide-based sensors and recognition elements. An example of this, is shown in our work on the use of these materials in actuating liquid crystals (see previous section of this report).

3) Carlini, A. S.; Adamiak, L.; Gianneschi, N. C. “Biosynthetic Polymers as Functional Materials” *Macromolecules* **2016**, *49*, 4379-4394

The third publication to appear in this reporting period related to bioconjugate polymeric systems is a review, appearing in Macromolecules. This work highlights advances in the field, and puts the work of many groups in context with respect to the goal of developing informational polymer systems through living polymerization methods, template syntheses and other efforts in sequence controlled polymerizations.

(PECASE) Biomolecular Programming of Discrete Nanomaterials for Sensors, Templates and Mimics of

SECTION 2: *In situ Liquid Cell TEM (LCTEM)*

Introduction

Transmission Electron Microscopy (TEM) and Scanning TEM (STEM) are extremely powerful techniques for characterizing nanomaterials due to the high spatial resolution, the ability to determine internal and 3D structures and the possibility of obtaining elemental information through the use of energy dispersive x-ray spectroscopy (EDS) and electron energy loss spectroscopy (EELS). Due to the high vacuum requirement of the microscope column, nanoparticles are not typically imaged under environmental conditions. For example, nanoparticles in solution are typically imaged through one of two techniques a) dehydration onto a TEM grid (dry state TEM) or b) vitrification of thin films of solution on a TEM grid (cryo-TEM).(11-14)

The first reports of TEM in liquids appeared over 70 years ago using both open(15) and closed(16) cell technologies. These two approaches still form the basis of all liquid EM techniques used today. However, both technologies lagged behind cryo-TEM in terms of structural characterization of nanomaterials in solution and this technique dominates the literature. Open cell environmental TEM (ETEM) uses differential apertures in order to create higher pressures very close to the sample allowing imaging in both liquids and gases. Prior to this century, open cell techniques were the most utilized method for environmental TEM imaging. By contrast, closed cell technology involves encasing the liquid or gas in a cell capable of mechanically withstanding the internal vacuum of the microscope and thin enough to allow the beam to fully penetrate (Figure 7). The cells are difficult to construct and the technique remained largely unused until a decade ago, when Ross *et al.* reported the first silicon nitride closed liquid cell for TEM.(17) These silicon nitride cells now form the basis of most liquid TEM measurements made, largely due to their commercialization.

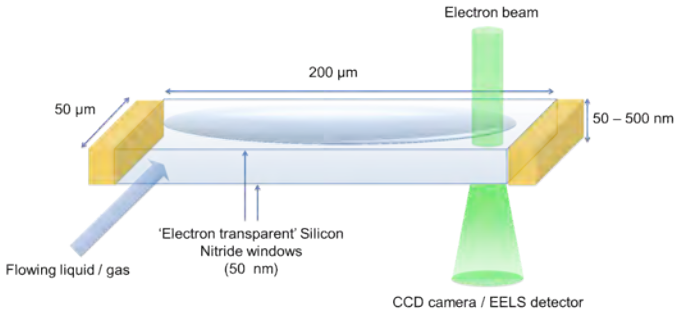

Figure 7. A schematic for an *in-situ* liquid TEM cell

Summary of Impact and Importance of Work in our Laboratory Related to LCTEM

Pioneering the use and development of liquid cell transmission electron microscopy (LCTEM) for the characterization of nanoscale dynamics with a focus on soft materials and/or organic-inorganic hybrid materials. This work includes an interest in the challenge of examining mechanisms of particle growth and formation with nanoscale resolution, but within the particles' native environment, within liquids. We have a particular interest in optimizing and adapting the methodology to allow imaging of

biological processes and biological nanomaterials both natural and semi-synthetic for the purpose of understanding fundamental properties of these materials in real time on the nanometer length scale.
Recent Publications:

a. Proetto, M. T.; Rush, A. M.; Chien, M. –P.; Abellan Baeza, P.; Patterson, J. P.; Thompson, M. P.; Olson, N. H.; Moore, C. E.; Rehingold, A. L.; Andolina, C.; Millston, J.; Howell, S. B.; Browning, N D.; Evans, J. E..; **Gianneschi, N. C.** "Dynamics of Soft Materials Captured by Transmission Electron Microscopy" *J. Am. Chem. Soc..* **2014**, *136,* 1162-1165. PMID: 23944844.
b. Patterson, J. P.; Abellan, P.; Denny, M. S.; Park, C.; Browning, N. D.; Cohen, S. M.; Evans, J. E.; Gianneschi, N. C. "Observing the Growth of Metal-Organic Frameworks by In Situ Liquid Cell TEM" *J. Am. Chem. Soc.* **2015**, *137*, 7322-7328.
c. Patterson, J. P.; Parent, L. R.; Cantlon, J.; Eickhoff, H.; Bared, G.; Evans, J. E.; **Gianneschi, N. C.** "Picoliter Drop-On-Demand Dispensing for Multiplex Liquid Cell TEM" *Microscopy and Microanalysis* **2016**, *22*, 507-514.

Our overarching goal is to develop liquid TEM for analyzing soft, dynamic materials of all kinds. Our research over the past several years has been pioneering in this field. We perceive that several key barriers exist to achieving this in general. These concerns include controlling, understanding, quantifying, and mitigating beam damage. In addition, we wish to design new instrumentation and methodologies that allow for mixing of multiple components within the cell allowing for chemical reactions and physical transformations for the first time. In addition, there is a serious data analysis issue, both in terms of real time, inline particle tracking, and data storage. Our work to date has addressed all of these issues by taking a number of tracks. First, we have utilized metal-organic frameworks (MOFs) as a test material to establish beam damage parameters for self-assembled soft materials (Patterson, J. P.; Abellan, P.; Denny, M. S.; Park, C.; Browning, N. D.; Cohen, S. M.; Evans, J. E.; Gianneschi, N. C. "Observing the Growth of Metal-Organic Frameworks by In Situ Liquid Cell TEM" *J. Am. Chem. Soc.* **2015**, *137*, 7322-7328). Second, we have studied nanoparticle fusion events for completely soft materials: that is, polymeric organic micelles (manuscript in preparation – work described below). Thirdly, in each of these cases we have utilized advanced particle tracking analysis in collaboration with Prof. Chiwoo Park (Florida State University). Fourthly, we have developed a new technique for setting up chemical gradients, and therefore setting up reactions (Patterson, J. P.; Parent, L. R.; Cantlon, J.; Eickhoff, H.; Bared, G.; Evans, J. E.; Gianneschi, N. C. "Picoliter Drop-On-Demand Dispensing for Multiplex Liquid Cell TEM" *Microscopy and Microanalysis* **2016**, *22*, 507-514). At the time of writing this report, we have embarked on our next effort to pattern the liquid cells themselves to allow for chemical reactions in conjunction with the arrayer tool described in the *Microscopy and Microanalysis* contribution and in a patent describing these systems (2016-026: Low volume drop dispensing liquid cell electron microscopy sample preparation).

Summary of Metal-Organic Frameworks by Liquid Cell TEM (LCTEM) - Patterson, J. P.; Abellan, P.; Denny, M. S.; Park, C.; Browning, N. D.; Cohen, S. M.; Evans, J. E.; Gianneschi, N. C. "Observing the Growth of Metal-Organic Frameworks by In Situ Liquid Cell TEM" *J. Am. Chem. Soc.* **2015**, *137*, 7322-7328

Metal-organic frameworks immediately came to mind as a material for analysis by LCTEM as a material that consisted mostly of purely organic material, but where the crystallinity would make it possible to observe beam damage, and/or growth of the materials in the liquid cell. This would essentially serve as a beam sensitive starting point in our ongoing efforts to study these materials.

Metal-organic frameworks (MOFs) are materials comprised of inorganic nodes (metal ions or metal ion clusters often referred to as secondary building units, SBUs) bridged by multitopic organic linkers.(18-23) MOFs are highly porous materials and are highly tunable by selection of the precursor components or post-synthetic methods.(24) MOFs have attracted great attention as materials for gas storage,(22, 25) separation,(26) catalysis,(21, 27) and for a range of other uses.(20) Despite the broad utility and interest in these materials, to date, there have been few studies on MOF nanoparticle self-assembly (spontaneous association of ligand and metal to form a unit cell) or growth (the propagation of the unit cell to form a nanoparticle), partly due to difficulties in analyzing the formation of the nanocrystals as they assemble and precipitate from solution. This lack of information leaves a large gap in our understanding of the underlying mechanisms and how to go about precisely controlling and tuning the porosity, or final morphology. Attfield et al. studied MOF growth by liquid atomic force microscopy (AFM),(28-31) which elegantly showed growth of selective crystal faces with high spatial resolution of their three-dimensional (3D) topographical structure. However, AFM has limited lateral and temporal resolution and is only surface sensitive. Consequently, the growth was observed on preformed MOF ‘seeds’ using dilute solutions. This prevented the observation of nucleation and subsequent growth kinetics. Therefore, we hypothesized that LCTEM would provide a unique, complementary analytical tool for studying MOF formation and providing insight into nucleation, internal rearrangement, or densification. Indeed, we did show that LCTEM can be used to observe the growth of MOFs at high magnification and in real-time, giving unique information for individual particles. Importantly, the observed growth rates and crystal structures match those obtained by standard synthetic conditions and bulk solution methods. Moreover, they serve as a model system for observing beam sensitive materials by this nascent technique. As shown in Figure 2, we have been able to observe growth kinetics and gain insight into processes occurring during damage to the MOF as well as crystallization.

Ongoing work on this project involves the observation under ambient conditions of these materials absorbing gases, and liquids as guests. In addition, we aim to observe crystal grown processes on various interfaces and surfaces.

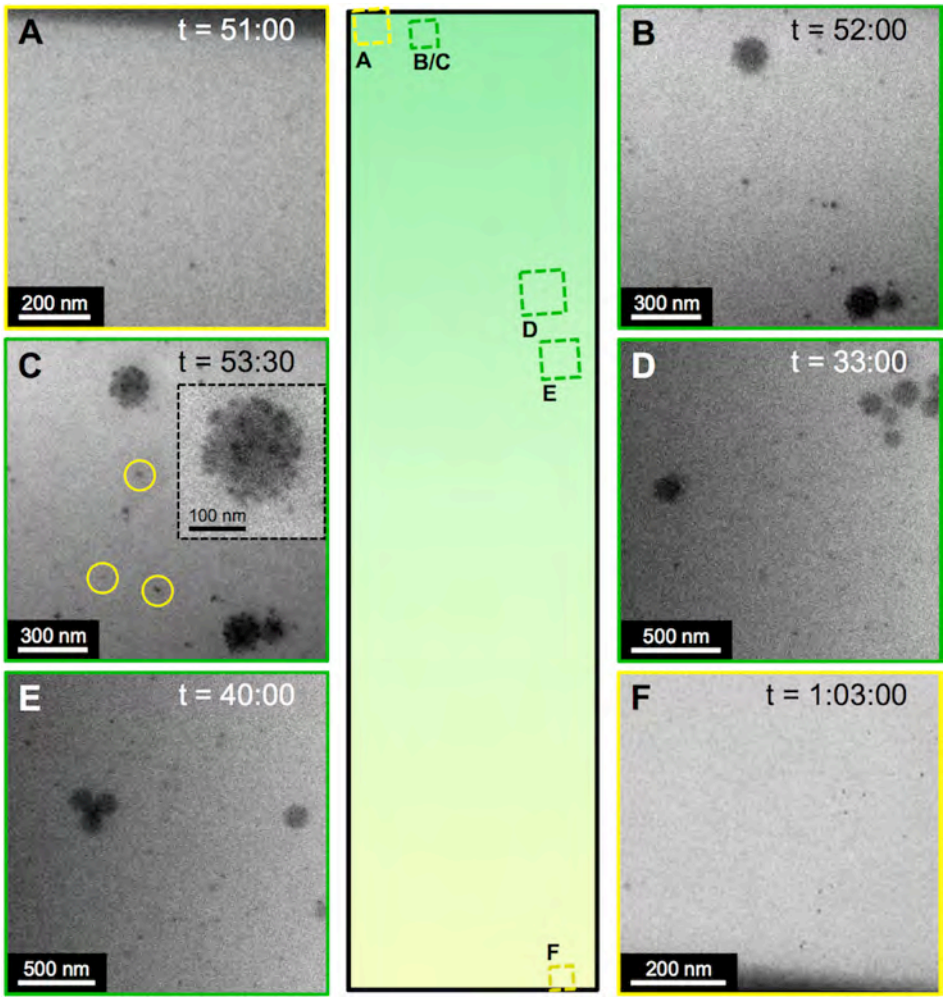

Figure 8. TEM images of the liquid cell after full diffusion and mixing of the UiO-66 (MOFS: blue) and Au NPs (yellow) has occurred. The images show significant diffusion of Au NPs into the UiO66 end of the cell (A-E) and little or no diffusion of the MOFs into the Au end of the cell (F). t = the time after sealing the liquid cell. The tall-narrow graphic in the center is a qualitative scheme of the liquid composition within the window region as observed 30 minutes after sealing the cell. Yellow is pure Au NPs, blue is pure UiO-66 MOF and green is a mixed composition of Au and MOF (now the primary composition). Labeled squares indicate the position on the window area where the respective TEM images (A-F) were acquired. Image C was acquired at the same location as B, 90 seconds later. Yellow circles in C indicate Au nanoparticles that have diffused into the field of view and stuck to the top or bottom window during the 90 second time period from image B.

Establishing chemical gradients in the liquid cell experiment for TEM - Patterson, J. P.; Parent, L. R.; Cantlon, J.; Eickhoff, H.; Bared, G.; Evans, J. E.; Gianneschi, N. C. “Picoliter Drop-On-Demand Dispensing for Multiplex Liquid Cell TEM” *Microscopy and Microanalysis* **2016**, *22*, 507-514

Liquid Cell Transmission Electron Microscopy (LCTEM) is bringing about a paradigm shift in the analysis of nanomaterials in solution. For the first time, we can use electron microscopy to not only characterize critical features including particle size and morphology but to observe liquid phase dynamics, in real-time with nanometer resolution.(17, 32) LCTEM has shown great potential for advancing our understanding of nanoparticle growth,(33-39) and particle-particle interactions.(40) There has been a particular focus on inorganic nanocrystalline materials such as Pt, and Pd because they provide high contrast and the ability to undergo electron beam induced growth starting with initiation of metal complex reduction during the imaging experiments.(34, 35, 37, 38)

In a typical LCTEM experiment, a liquid sample can be deposited onto the surface of a flat silicon nitride chip (ca. 2.5 x 2.5 mm square) and subsequently sealed from the external environment (i.e. the internal vacuum of the electron microscope) by placing a second chip on top of the solution and enclosing the chips within a liquid cell TEM holder.(32) The liquid thickness of the cell is therefore set by the size of any nanoparticles within the sample, which physically hold the chips apart. If a thicker cell is required, so-called 'spacer-chips', which have raised columns on the silicon nitride surface can also be used to physically separate to silicon nitride surfaces. These spacer-chips also allow for the cells to be assembled in air, and liquid to be flown into the windows after insertion into the microscope.

While many reports discuss the great potential LCTEM will have in the study of nanoparticle systems formed though the mixing of solutions containing various required components or conditions,(32, 41) until the effort reported here, there was no demonstration whereby two solutions have been mixed within the viewing windows of the liquid cell; that is, no reaction had been demonstrated within the transmission electron microscope itself. We contend that this has largely been due to an inability to control the dispensing and flow of separate liquids within the low volume cell. Furthermore, while several commercial holder designs in theory, allow multiple liquids to be flowed into the *in situ* TEM holder, mixing occurs in the collection wells and not directly between the chips.(42) This means the process is unreliable at best, and at worst will very likely never occur in any meaningful fashion.

In this work we demonstrated that picoliter (pL) drop-on-demand dispensing technology can be used to controllably load multiple samples onto a single liquid cell window, which provides an opportunity to create both high throughput liquid cells as well as controlled mixing of multiple different solutions (Figure 8). We demonstrated this by applying separate solutions of gold nanoparticles (Au NPs) and nanocrystals of the metal-organic-framework (MOF), UiO-66 to a single liquid cell window where initial mixing occurs upon assembly of the cell and diffusion of components continues during TEM imaging. We propose that this novel LCTEM technique will open the door for *in situ* nanomaterial synthesis studies that require the mixing of solutions directly in the viewing area, and for studies of responsive nanomaterials that undergo dynamic transformations upon mixing to change solution conditions and/or constituents.

These experiments demonstrated that automated picoliter drop-on-demand dispensing, combined with automated grid recognition and alignment in the sciTEM instrument can be used to mix samples within the liquid cell, allowing nanoparticles to diffuse and interact while imaging in the microscope. Furthermore, using this dispensing technology and imaging strategy, one can conceive of many array designs where the mixing time of multiple different solutions could occur within one experiment. From a fundamental standpoint, technology for controlling the dispensing of low liquid volumes is essential for the advancement of LCTEM and this proof-of-concept shows the great potential to perform direct solution mixing and/or high-throughput *in situ* experiments. We intended this study together with the published work and patent on the subject as an initial demonstration of an approach that should

enable researchers to study processes involving mixing of materials and/or reagents. In addition, the work should set the stage for the design and fabrication of novel chip designs to fully take advantage of using picoliter drop-on-demand dispensing techniques in combination with automated grid alignment in order to controllably load and mix solutions within the liquid cells.

Liquid Cell TEM for the Analysis of Micellar Nanoparticles Undergoing Phase Transitions – Manuscript in Preparation

The behavior and phase changing nature of soft matter in water is a key step in the formation of complex biological and synthetic materials. For block copolymer (BCP) assemblies, a delicate interplay exists between the kinetic and thermodynamic parameters, which govern their behavior in solution. There have been great efforts made to characterize the structural evolution of BCP assemblies, principally via *in situ* bulk scattering methods or *ex situ* microscopy. *In situ* scattering experiments are typically performed on simple systems e.g. special micelles, providing a bulk overview of the sample dynamics, such as average micelle size or shape evolution. *Ex situ* microscopy is preferred for more complex structures, but is incapable of revealing the underlying dynamics and mechanisms of morphological transformations. Consequently, while highly complex structures can now be formed through BCP assembly, our ability to directly monitor these materials has not significantly improved in the last several decades. This has left a huge understanding gap, and even for the simplest BCP structure, the spherical micelle, it is unclear exactly how these structures assemble and evolve.

To expand the fundamental understanding of complex soft material evolution, direct *in situ* observations with the appropriate spatial and temporal resolution are clearly needed. Liquid Cell Transmission Electron Microscopy (LCTEM) provides such a platform, allowing real-time imaging of nanomaterial morphologies and dynamics in liquids with nanometer spatial resolution. Here, through the use of LCTEM videography, we show clear evidence of a morphology switch and growth process in kinetically trapped BCP assemblies, from spherical micelles into larger, bicontinuous micelles. This process occurs through multiple simultaneous pathways, which exist over all particle size regimes, including particle-particle fusion (a process which is often dismissed due to the high energy barrier requirements) and unimer addition. The ability to monitor the evolution of individual particles in real time with nanometer spatial resolution allows us to quantify the kinetics of individual micelles, track the transition states of fusion events, non-fusion particle-particle interactions, and find a new oscillatory growth behavior, which would not be possible by bulk scattering or *ex situ* microscopy techniques.

(PECASE) Biomolecular Programming of Discrete Nanomaterials for Sensors, Templates and Mimics of

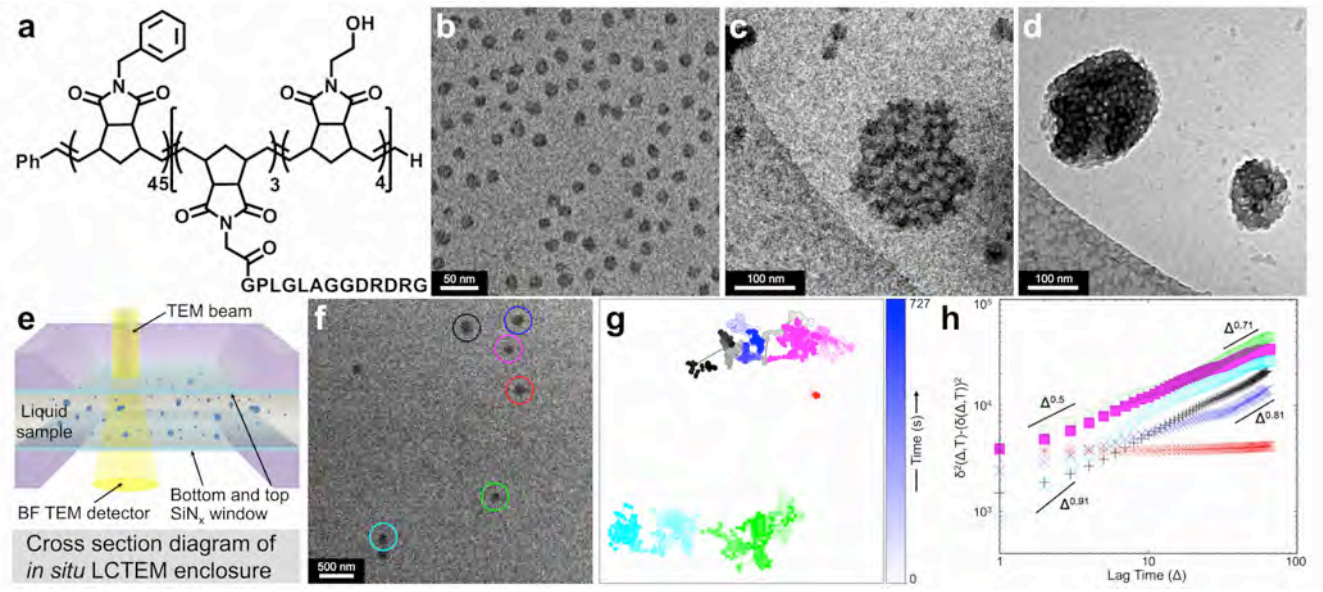

Figure 9. BCP structure, cryoTEM images of as-assembled and post-agitated BCP micelles in aqueous buffer solution, and general overview of LCTEM experimental set-up and data obtained in LCTEM experiments with this micelle system.

The spherical micelles we study here were initially formed by solvent switch from dimethylformamide into a PBS buffered aqueous solution (followed by extensive dialysis into pure PBS buffer) of zwitterionic phenyl-*b*-peptide amphiphilic block copolymer (Figure 9a). The micelles were characterized by cryo-TEM (Figure 9b) and dynamic light scattering, DLS, which produced consistent particle size and morphology results of well-defined 19 ± 2.5 nm diameter micelle nanospheres (aggregation number, N_{agg} ~280), where individual polymer chains are likely radially arranged within the micelle spheres with hydrophobic phenyl cores and hydrophilic peptide coronas. Physical perturbation of these micelles (e.g. vortexing or controlled evaporation) results in the reorganization of this system into a larger size distribution of particles (diameters on the order of 50-200 nm) that show a bicontinuous structure by cryo-TEM (Figure 9c-d). Analysis of the initial micelles solution in the absence of perturbation over several months reveals no size or morphology change, and after perturbation the system does not relax back to the original form, indicating that the original micelles structures were kinetically frozen.

The *in situ* LCTEM imaging experiments were performed by loading a sub-μL volume of the original spherical micelle solution between two glow-discharged SiN_x membrane windows in a commercial liquid flow TEM holder, as illustrated in Figure 9e. The microscope was aligned for low-dose operation, and five different dose rates were used during observation in order to determine the effect of the electron beam on the sample and to achieve different image magnifications.

When the e^- beam was first turned on at the start of LCTEM imaging, a distribution of larger sized micelles was observed (~40 nm up to 200 nm in diameter). The act of physically loading the sample into the liquid stage enclosure has the potential to slightly alter the solution chemistry/concentration, and to apply local pressure variations and shear forces that we believe has triggered the morphology

switch and size we see at the start of LCTEM imaging, which then continues during the course of the LCTEM experiment. We believe the micelle nanospheres observed during the LCTEM experiment have similar bicontinuous micelle structures found in the *ex situ* perturbation experiments (Figure 9c-d), comprised of both internal water and polymer phases.

Using a multi-object tracking algorithm (MOTA, **in collaboration with Prof. Chiwoo Park, Florida State University*), all individual objects in each raw LCTEM video (Figure 9f is one example) have been thresholded and center-of-mass tacked to determine an x,y location (Figure 9g), area measurement, major and minor diameter measurement for each micelle in every video frame. Through collaboration with Prof. Francesco Zerbetto and Dr. Evangelos Bakalis *(University of Bologna, Italy)*, we compute the time moving mean average variance of displacement (TMAVD) and classify the stochastic mechanisms that describe each micelle's motion. Analysis by the method of generalized moments (structure function) finds a multi-fractal nature in the stochastic mechanisms of motion for all 56 discrete micelles observed in LCTEM experiments, which is generated by interplay between fractional Gaussian noise (fGn) and Truncated Levy Walks or a more complicated mechanism. Micelle motion is generally sub-diffusive (D_a ~10^3-10^4 nm^2/s^a) with variations in sub-diffusion exponent (*a*) as a function of lag time (Figure 9h) and some tendency to confinement of the motion is apparent. The general structure function for these micelles, primarily fGn, has been identified with the operative mechanisms that drive the motion of a number of experimental and theoretical studies in living cells and lipids, and reflects either the presence of a viscoelastic environment, or of a crowded environment with random obstacles that are not interacting with each other, which seems highly consistent with expected environment within the liquid cell. The analysis shows that at the lowest dose rate, a significant number of particles (10) are either partially or fully trapped, which is not seen at either of the higher dose rates. Additionally, for increasing dose rates, a larger fraction of micelles follow a consistent sub-diffusive motion with exponents significantly higher than for lower doses. This shows that although the beam does not directly affect the overall motion of the particles, secondary effects, such as beam induced changes in how the micelles interact with the surface, are present. Interestingly, cross-correlation analysis of particle surface area (*s*) and step size (*l*), shows there is no relation between each individual micelle's dynamics and its average size or any changes in its size over time.

Figure 10a-f shows series of single frames from a LCTEM video where two of the micelles in the field of view undergo an explicit fusion event, to coalesce into a single, larger sphere. The plots of the area, major and minor diameter, and eccentricity (aspect ratio) for the two fusing particles (red and blue) and the single particle after fusion (black) are displayed in Figure 10g,h,i respectively. At the beginning of the video, the red and blue micelles are separated by several microns in lateral distance and approach each other over time by sub-diffusive FBM driven by fGn. The area of red micelle is roughly double that of the blue micelle, but they have very similar spherical morphologies and measured eccentricity aspect ratios (~0.7). At t = 142 s (Figure 10c), the two micelles first touch and we can begin to analyze the transition state of a single fusion event. The process of fusion begins through neck formation, and over the subsequent ~120 s the coalesced particle undergoes a process of relaxation (Figure 10d,e), as its eccentricity increases from an initial value of ~0.2 when the two

micelles first meet, to a stable plateau of ~0.75. During this period of morphological transformation, the projected area of the particle decreases and stabilizes, as the volume of the two fusing micelles distributes more evenly in three-dimensional space into a generally spherical morphology. This likely occurs through a process of transport and reorganization of both individual polymer chains and the internal water phase by some combination of solid-state diffusion and viscous flow due to the complex solvent-polymer composite structure of micelles. Interestingly, the final relaxed volume of the black micelle is significantly greater than the sum of the volumes of the red and blue micelles (~24 % larger), suggesting that during the process of fusion and relaxation additional water phase is incorporated internally, such that the coronal blocks of the polymer chains are able to swell and stretch within the new larger diameter micelle, so that each chain occupies more space than they do in either of the initial smaller micelles. Alternatively, fusion might activate new hydration channels, altering chain swelling and the overall volume in space that the structure occupies.

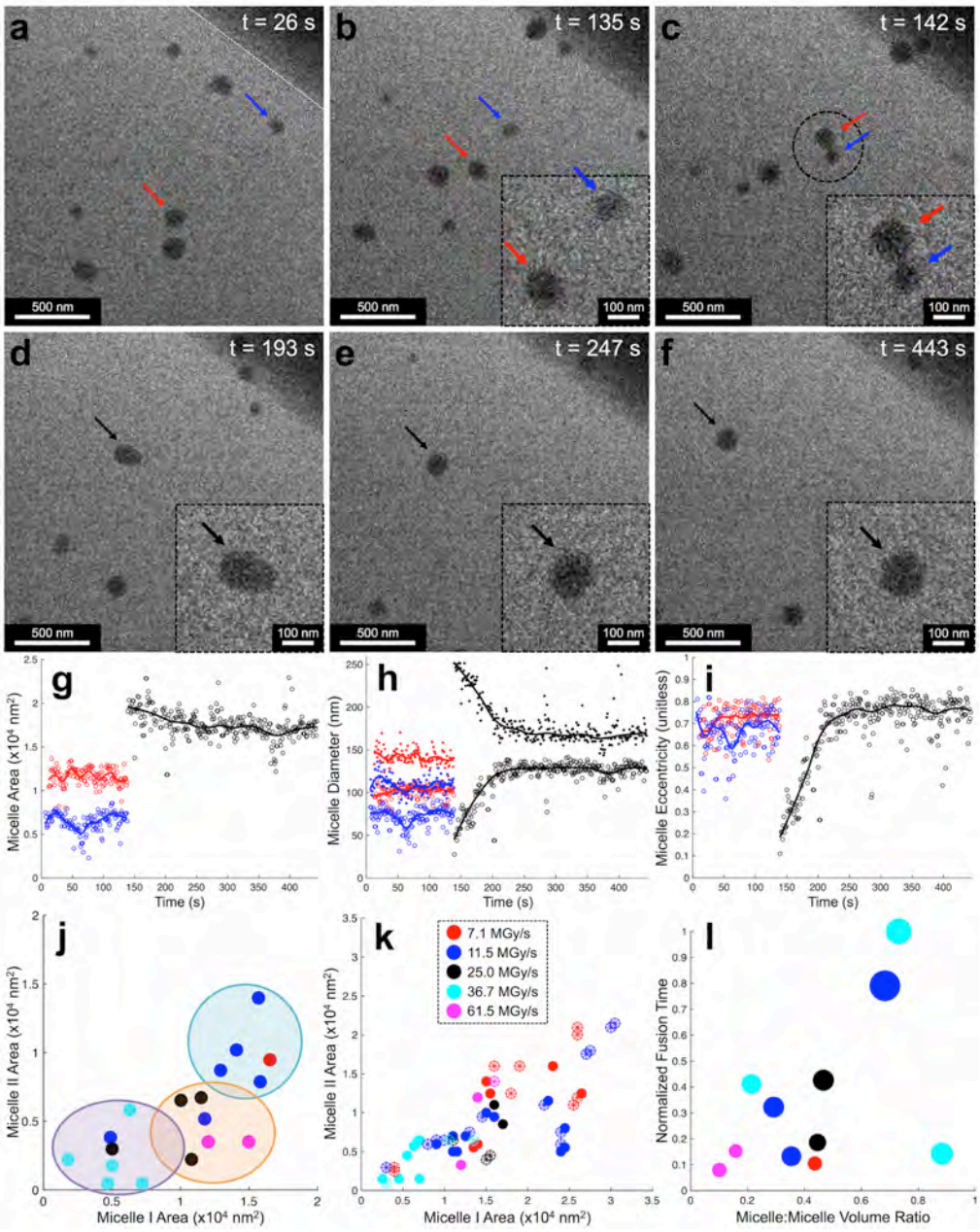

Figure 10. LCTEM data of single micelle-micelle fusion event, and statistical analysis of all observed fusion events

In total, 19 separate fusion events were directly observed during the LCTEM experiment involving a wide range of pre-fusion micelle sizes, and micelle-micelle pair ratios. Figure 10j plots each fusion event as a function of the pre-fusion area of the two fusing micelles. Fusion events are distributed over a broad micelle-size range, and can be roughly divided into three regimes; fusion between two large micelles (teal oval), fusion between one large micelle and one small micelle (orange oval), and fusion between two small micelles (purple oval). This finding diverges from the process of micelle

fusion proposed by Epps et al., which was suggested to primarily involve the smallest spherical micelles, forming highly unstable intermediates, which then rapidly fuse with other small micelles to become stable large spherical micelles. We instead find that fusion occurs for essentially all micelle sizes in this system, and furthermore, that any individual fusion event is infrequently followed by an immediate additional fusion event.

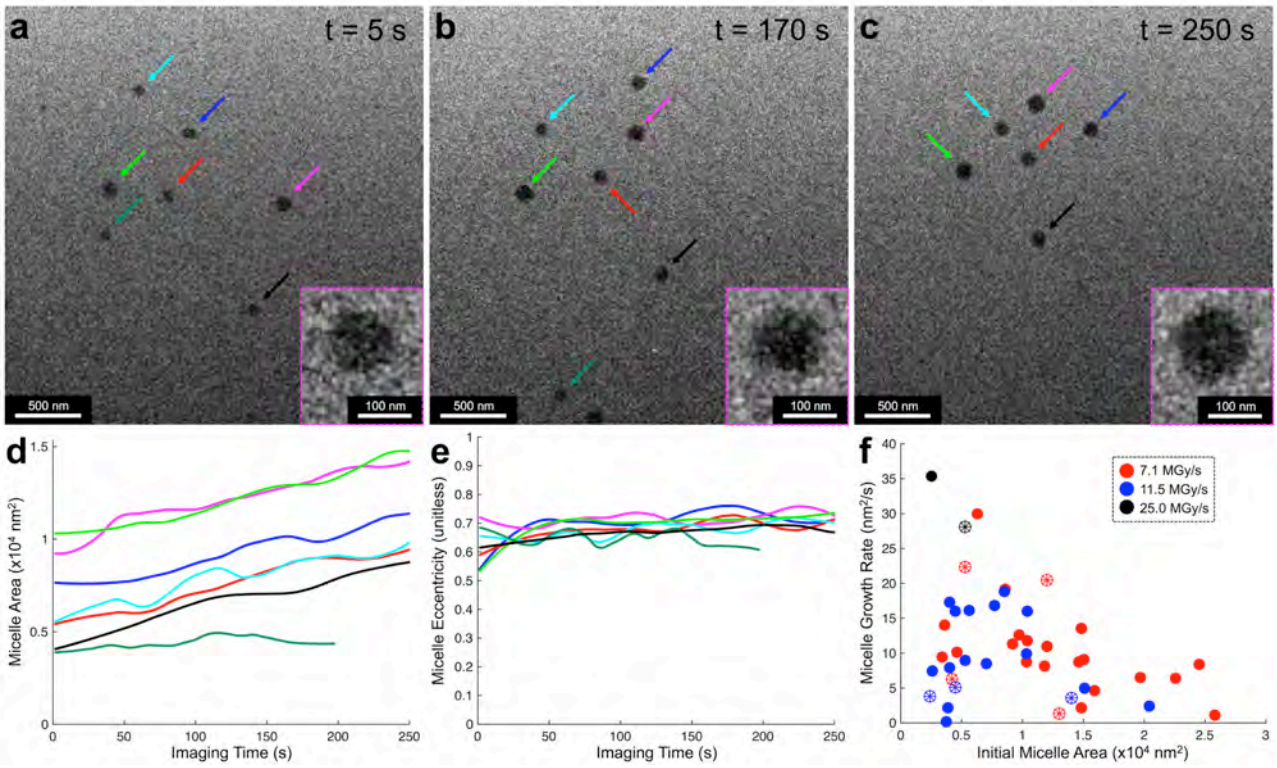

Figure 11. LCTEM data of individual micelle growth attributed to a process of unimer addition.

In addition to size evolution by a micelle-micelle fusion pathway, we also observe individual micelle growth in the absence of fusion or aggregation events (Figure 11). We attribute this isolated growth to a process of unimer attachment and insertion of solvated free polymer chains, or small clusters of polymer, into the micelle structure. Thought the CMC of this system at quiescent conditions is known to be very low (i.e. very little free unimer relative to the number of micelles in a given volume), we believe that micelle breakup during the liquid cell assembly process, either induced by compressive pressure of shear force applied during loading or by the very large air-liquid interface when the solution is first applied, has generated an appreciable concentration of free unimer (not assembled in to macromolecular micellar structures) that preferentially adsorb and accumulate at the SiN_x surfaces of the cell. Charging of the SiN_x membrane, or the adsorbed unimer chains, by the e^- beam during LCTEM imaging could induce unimer to release from the window surface and become free in solution locally in higher concentrations than the CMC of the bulk solution, which drives the process of insertion in to the existing micelle aggregates, leading to the observed gradual micelle growth.

Figure 11a-c shows a series of frames from one LCTEM video where micelles in the field of view clearly exhibit a continuous, gradual mode of individual growth over time. The area and eccentricity (aspect ratio) of the seven micelles are plotted as a function of imaging time in Figure 11d and 11e respectively. We have tracked and quantified the micelle area over time for each particle imaged continually for longer than 180 s for all the LCTEM videos. The scatter plot in Figure 11e displays each micelle as a single data point, with its linear-fit unimer attachment growth rate as a function of the initial micelle area. There is an overall inverse trend of growth rate with micelle size, where smaller micelles on average grow more rapidly than larger micelles. However, several of the smallest micelles break from this trend, exhibiting little to no growth via a non-fusion driven mode.

In summary, low dose LCTEM allows for unperturbed observations of never before seen nanoscale morphology changes and phase transitions. This study is the first of its kind, pointing a way forward towards a new approach to studying nanomaterials in general.

SECTION 3: *Synthetic Melanosomes and Melanin-like Materials*

Introduction

from the SCENEs

A selection of stories from C&EN's six online TOPICAL NEWS CHANNELS

FROM THE NANO SCENE

SYNTHETIC MELANIN FILMS MIMIC BIRD PLUMAGE

The bright hues of some birds' feathers arise from structural color—light-reflecting patterns formed by the orderly arrangement of nanoparticles containing the pigment melanin. Now, by using nanosized spheres of polydopamine, a synthetic polymer that acts like melanin, scientists have created films that closely mimic the pure blues, greens, and reds found in many avian feathers (*ACS Nano* 2015, DOI: 10.1021/acsnano.5b01298). Such colored films could be used in optical sensors, fade-resistant paints, or ultraviolet-protective coatings. Nathan C. Gianneschi of the University of California, San Diego; Matthew D. Shawkey and Ali Dhinojwala of the University of Akron; and colleagues polymerized dopamine to form 150-nm-diameter spheres. They suspended these nanoparticles in water, then dried them on silicon wafers to produce 1-cm² films in colors spanning the spectrum from blue to red. Each film reflected a narrow range of wavelengths—determined by its thickness—to produce pure colors. In red films, for example, 95% of the reflected light was between 600 and 700 nm. Other methods, such as spin-coating, may allow the researchers to increase the size of the films.

Films made with polydopamine nanoparticles span a range of colors.

ACS NANO

Over the past several years, our group has developed synthetic methods for the preparation of synthetic melanin nanoparticles. These efforts have lead to several published article in collaboration with Matthew Shawkey at Akron University over the past several years on the development of synthetic approaches towards utilizing synthetic melanin nanoparticles to build structural color elements. This work appeared in ACS Nano (Xiao, M.; Li, Y.; Allen, M.; Deheyn, D.; Yue, X.; Zhao, J.; **Gianneschi, N. C**.* Shawkey, M.;* Dhinojwala, A.* Bioinspired Structural Colors Produced via Self-Assembly of Synthetic Melanin Nanoparticles. *ACS Nano*, **2015**, *9,* 5454-5460). This paper has

garnered significant press recognition, and more than any of our other papers, has garnered the attention of the more popular press. This has included articles in *Popular Science Magazine*, *The Scientist,* and in *C&E News* (see figure inset on previous page and at http://cen.acs.org/articles/93/web/2015/05/Synthetic-Melanin-Films-Mimic-Colors.html). In addition, the work was described in terms of sense-response switchable color switches in a recently published article (Xiao, M.; Li, Y.; Zhao, J.; Wang, Z.; Gao, M.; Gianneschi, N. C.; Dhinojwala, A.; Shawkey, M. D. "Stimuli-Responsive Structurally Colored Films from Bioinspired Synthetic Melanin Nanoparticles" *Chemistry of Materials* **2016**, *28*, 5516-5521). In this work we presented, for the first time, the preparation and assembly of well-defined synthetic melanin nanoparticles as mimics of natural arrays of melanosomes used frequently in bird feathers to generate structural coloration. The work will be of interest to the general materials science community including those interested in bio-inspired nanostructures, structural color, polymeric nanomaterials, surface chemistry, sensor design and functional coatings.

Summary of Impact and Importance of Work Related to Melanin-like Materials

Development of melanin-based materials – synthetic methodologies, physical characterization and functional applications. In these studies we have sought to elucidate basic properties including metal ligand interactions, magnetic properties, and the possibility of mimicking nature's mechanism for producing structural color in birds. This work represents initial investigations that seek to elucidate the basic function of these materials and the mechanisms by which they give rise to structural color, how that may be programmed and switched, and how the may be used as catalytic and magnetic materials.

Recent Publications:

a. Xiao, M.; Li, Y.; Allen, M.; Deheyn, D.; Yue, X.; Zhao, J.; **Gianneschi, N. C**.* Shawkey, M.;* Dhinojwala, A.* Bioinspired Structural Colors Produced via Self-Assembly of Synthetic Melanin Nanoparticles. *ACS Nano*, **2015**, *9,* 5454-5460 Electron Microscopy" *J. Am. Chem. Soc..* **2014**, *136,* 1162-1165. PMID: 23944844.
b. Xiao, M.; Li, Y.; Zhao, J.; Wang, Z.; Gao, M.; **Gianneschi, N. C.**;* Dhinojwala, A.;* Shawkey, M. D.* "Stimuli-Responsive Structurally Colored Films from Bioinspired Synthetic Melanin Nanoparticles" *Chemistry of Materials* **2016**, *28*, 5516-5521

Summary of UV-Protective Qualities of Synthetic Melanin-like Nanoparticles as Mimics of Naturally Occuring Melanin-carrying organelles, or Melanosomes – Manuscript in Review

One particular direction, in addition to responsive color elements, is the ability of these materials to help protect skin cells from UV-light. A primary role for melanin in skin is the prevention of UV-induced nuclear DNA damage to human skin cells, where they serve to screen out harmful UV radiation. Melanin is delivered to keratinocytes in the skin after being excreted as melanosomes from melanocytes. Defects in melanin production in humans can cause diseases, which currently lack effective treatments, because of their genetic origins, leading in turn to subsequent diseases (i.e. skin cancer). Their widespread prevalence and an increasing interest in the performance of polymeric materials of various kinds related to melanin has led to synthetic routes for preparing melanin-like materials. Melanin-like nanoparticles (MelNPs) can be synthesized via spontaneous oxidization of

dopamine, yielding materials that are biocompatible. In this work, we aimed to explore MelNPs as synthetic analogues of naturally occurring melanosomes by studying their uptake, transport, distribution and UV-protective capabilities in human keratinocytes. MelNPs are endocytosed, undergo perinuclear aggregation and form a supranuclear cap in human epidermal keratinocytes (HEKa) mimicking the behavior of natural melananosomes. We have been able to demonstrate that synthetic MelNPs so dispersed within keratinocytes, can serve to protect the cells from UV damage.

Natural melanins are found across the animal and plant kingdoms, where they perform various biological functions, including in photoprotection, photosensitization, free radical quenching, metal ion chelation, and in the central nervous system of humans. There are several types of melanin that exist in the human body, including eumelanin, pheomelanin and neuromelanin. Eumelanin is the most common type among them, primarily determining the color of human skin. More importantly, it is able to prevent UV-induced nuclear DNA damage of human skin cells by screening out harmful UV radiation. Solar UV radiation is absorbed by DNA and damages nuclei in epidermal cells, which can lead to the formation of mutations and subsequent, irrecoverable damage. In the basal layer of the epidermis, specialized melanocytes produce the melanin containing organelles, termed melanosomes, in which melanin is synthesized and deposited. In skin, melanosomes are transferred from melanocytes to neighboring keratinocytes to form perinulcear melanin caps. The melanosomes accumulate around the nuclei in the form of melanin caps for the mitigation of UV damage to DNA. Indeed, people are generally familiar with the process by which exposure to UV-radiation causes melanogenesis, observed as a change in skin color commonly referred to as tanning. The integrated biological system for the induction, production, transfer and degradation of melanosomes is significant for the health of human skin, with melanin-defective diseases, such as vitiligo and albinism highlighting the importance of these processes. Vitiligo is caused when the immune system wrongly attempts to clear normal melanocytes from the skin, effectively stopping the production of melanosomes. Albinism is caused by genetic defects causing the failure of a copper-containing tyrosinase involved in the production of melanin. Both diseases lack effective treatments and they both promote significant risk of skin cancer in patients.

Water-dispersible, melanin-like nanoparticles (MelNPs) can be synthesized, demonstrating high biocompatibility making them potentially suitable for various biomedical applications, including as iron-chelated T_1-weitghted MRI contrast agents, serving as surface modification of other nanostructures for water-dispersible enhancement, and targeted therapeutic and bioresponsive nanoprobe applications. Synthetic MelNPs are prepared via the spontaneous oxidative polymerization of dopamine under alkaline conditions in aqueous solution. By contrast, biosynthetic melanins are formed in epidermal melanocytes involving tyrosinase-catalyzed oxidative polymerization of tyrosine, giving rise to black, insoluble eumelanins. Both synthetic and biosynthetic melanins appear to consist of largely planar oligomeric scaffolds. MelNPs can be prepared in a variety of sizes and shapes, including spheres, nanorods, and hollow spheres. These various morphologies of melanin nanoparticles are prevalent in nature such as in bird feathers where they play a shape and packing dependent role as iridescent structural color elements. However, extraction of melanins from natural sources can be problematic and far more complex than direct synthesis of them in the laboratory.

Therefore, synthetic melanins have been widely used as models for exploring the function and mechanism of natural eumelanins. For example, our own work on MelNPs described above and in our ACS Nano paper has shown that synthetic forms can be used to mimic the performance of bird feathers in terms of structural coloration, and the materials themselves can be prepared in a facile and precisely controllable manner.

We hypothesized that synthetic MelNPs would mimic naturally occurring melanosomes, and be taken up by keratinocytes in cell culture in turn providing photoprotection by adopting the same kind of perinulcear melanin cap in human epidermal keratinocytes as is observed for natural melanin. This hypothesis is predicated on the fact that the process of transfer of melanosomes from melanocytes to keratinocytes can occur when these two cell types are co-cultured *in vitro*. To test our hypothesis, we first synthesized spherical MelNPs by spontaneous oxidization of dopamine under alkaline conditions, introducing aqueous ammonia to an aqueous solution of monomers (Figure 12a). The resulting spherical MelNPs showed narrow size distribution around 200 nm, with excellent size homogeneity, demonstrated by dynamic light scattering (DLS), transmission electron microscopy (TEM) and scanning electron microscopy (SEM) (Figure 12c-d). Moreover, Energy Dispersive X-ray (EDX) measurements demonstrated that the elemental composition (C, N, O) and distribution in MelNPs is theoretically the same as natural eumelanin. Additionally, the Fourier transform infrared (FTIR) spectroscopy of MelNPs showed signals consistent with natural eumelanin including carboxylic acids (1038 cm^{-1}), hydroxyls (3225 cm^{-1}), -C=O (1617 cm^{-1}), -C=C- bond (2156 cm^{-1}) and -C-N= bond (1402 cm^{-1}). Eumelanin in the condensed phase and in solution has well-known, broad-band monotonic absorbance, including in the ultraviolet and the visible spectrum. Aqueous solutions of MelNPs appeared black in color (Figure 12, inserted picture) with a broad absorption in the UV-vis spectrum from 250 nm to 850 nm [Figure 12b], which was consistent with eumelanin extracted from natural organelles. To get a more profound insight into the chemical structure of the particles, they were analyzed using MALDI-TOF mass spectrometry. The signals with high intensities revealed oligomeric structures of both 5,6-dihydroxyindole (DHI) and 5,6-dihydroxyindole-2-carboxylic acid (DHICA). Several other fragment structures were also found. Similar monomeric units have been observed previously by MALDI-MS analyses of natural sepia eumelanin. The combined results illustrate that the synthetic MelNPs exhibit chemical composition similar to natural eumelanin,.

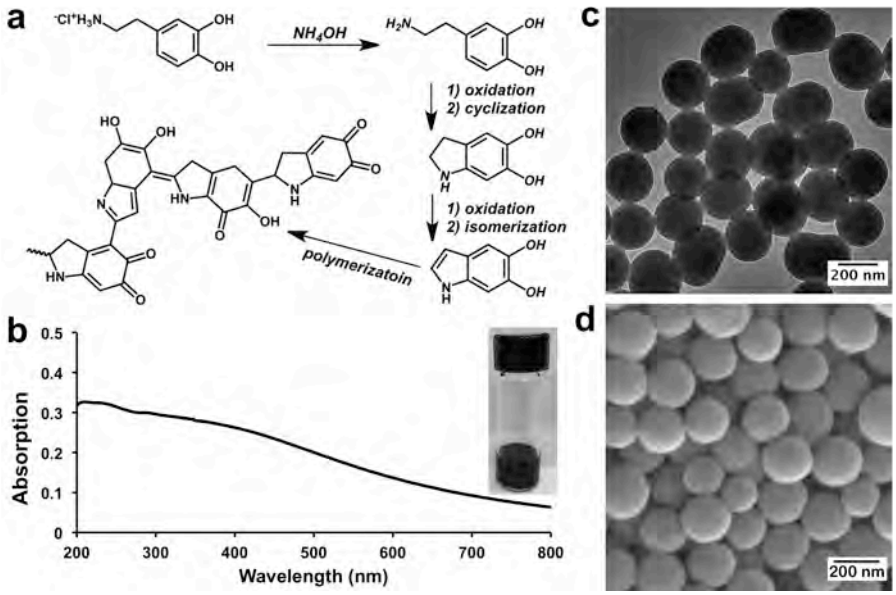

Figure 12. Synthesis and characterization of synthetic melanosomes. a) Synthetic scheme for the preparation of MelNPs; b) UV-vis spectrum for an aqueous solution of MelNPs. c) TEM image and d) SEM image of MelNPs.

Uptake of synthetic MelNPs into human epidermal keratinocytes (HEKa) was first examined with respect to the concentration-dependency and time-dependency of the process. With concentrations of 0.4 mg/ml, 0.1 mg/ml and 0.02 mg/ml, MelNPs were incubated with HEKa cells for 4 hours. TEM images indicated MelNPs were taken up into HEKa cells. However, some MelNPs tended to adhere to the cell membrane at high concentrations (0.4 and 0.1 mg/ml). Therefore, a concentration of 0.02 mg/ml was chosen for subsequent experiments. In a prior study, Ichihashi *et al.* extracted natural melanosomes from melanocytes and studied their interactions with keratinocytes. It was shown that the melanosomes are gradually degraded, leading to the melanin being dispersed around the nucleus of the keratinocytes asymmetrically in a process occurring over the time course of 24 hours. Therefore, to test whether MelNPs showed similar behavior, they were incubated at 0.02mg/ml, with HEKa cells and observed at 4 hours, 1 day, 2 days and 3 days (Figure 13). MelNPs were observed as black regions under brightfield confocal microscopy. At 4 hours the confocal images revealed MelNPs (black) surrounding the nuclei (blue), with others distributed in the cytoplasm, which was consistent with TEM data (Figure 13). However, after 1 day incubation, melanin is accumulated unevenly in the perinuclear area in a manner that appears consistent with the observations of natural extracted melanosomes. After 3 days incubation, the MelNPs showed clear signs of degradation (Figure 13a). Moreover, we observed that the degraded MelNPs and undegraded MelNPs exist in some HEKa cells simultaneously, which may be caused by the sequential order of uptake into cells. To examine whether these processes were inherent to the MelNPs within keratinocytes, we incubated them with mesothelial cells (MeT-5A), chosen as a control epithelial cell-type distributed within tissues that do not normally take up and process melanosomes. At the same time points MelNPs lacked any specific trafficking or localization indicating a random distribution in the cytoplasm. In addition, gold

nanoparticles (AuNPs) with a similar size and surface charge to the MelNPs, were incubated with HEKa cells, again showing random dispersion rather than specific localization (this data not shown here).

Melanosomes are tissue-specific lysosome-related organelles of pigment cells in which melanins are synthesized and stored. In epidermal melanocytes, melanosomes are ultimately transported to neighboring keratinocytes, which retain the melanin while in the basal layer and degrade as they move to the skin surface and differentiate. The melanosome is characterized as a lysosome-related organelle because melanin must be synthesized and polymerized with the help of enzymes and structural proteins within the organelle, where acidic pH seems to be required. We hypothesized the transportation and degradation of MelNPs was similarly driven by a lysosomal process in the HEKa cells. To test this hypothesis, we investigated the possible co-localization of lysosomes and MelNPs. We incubated MelNPs with HEKa cells for 4 hours, 1 day and 3 days, and used a specific dye to stain lysosomes (LysoTracker, Red DND-99, red). Indeed, confocal fluorescence microscopy images showed the co-localization of lysosome and melanin (Figure 13b). Therefore, MelNPs potentially utilize a similar pathway to natural melanosomes, undergoing lysosome-induced degradation and subsequent accumulation to form an artificial perinuclear cap (evident in Figure 13c). After 4 hours of incubation the MelNPs appear as clusters in the cytosol surrounded by a membrane (Figure 13a). After 3 days, MelNPs were observed by TEM, without a surrounding membrane in the cytosol and dispersed among keratin fibers (Figure 13d). Similar phenomena were observed when treating keratinocytes with extracted natural melanosomes, supporting our conclusion that the MelNPs perform as artificial melanosomes utilizing the same transportation and degradation pathway as natural melanosomes.

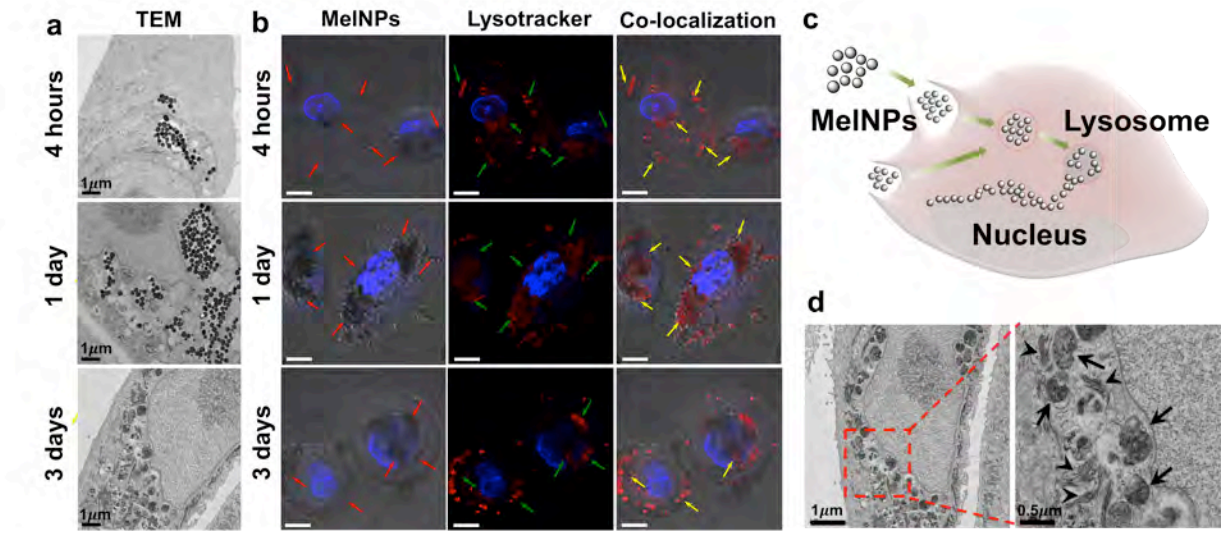

Figure 13. Imaging the uptake and cellular distribution of MelNPs in HEKa cells. a) TEM images for HEKa cells incubated with 0.02 mg/ml MelNPs for 4 hours, 1 day, and 3 days; MelNPs were uptaken inside HEKa cells and transported to the perinucleous area to form supranucleous caps; b) Confocal Laser Scanning Microscopy images for co-localization of MelNPs and Lysosome in HEKa cells. Nuclei of HEKa cells were stained by

Hoechst 33342 (blue); lysosomes were stained by LysoTracker Red DND-99 (red, indicated with green arrows); MelNPs were black in HEKa cells under bright field (indicated with red arrows); the co-localization of bright-field, black MelNPs and red fluorescence for labeled lysosomes are indicated with yellow arrows. Scale bars are 10 μm. c) Scheme for the uptake, transportation and accumulation of MelNPs in HEKa cells; d) Magnification of transmission electron microscopy image for HEKa cells incubated with 0.02 mg/ml MelNPs for 3 days. Melanosomes are indicated with black arrows, and keratin fibers indicated with black arrowheads.

DNA damage is the predominant mode of damage caused by UV radiation. UV radiation induces two of the most abundant mutagenic and cytotoxic DNA lesions known; cyclobutane-pyrimidine dimers (CPDs) and 6-4 photoproducts (6-4PPs) and their Dewar valence isomers. Therefore, we aimed to test for protective qualities of MelNPs by analyzing DNA damage in HEKa cells after treatment with MelNPs followed by UV irradiation (Figure 3). In mammalian cells, damage to genomic DNA can be lethal, inducing the formation of phosphorylated H2AX.(REF) Therefore, DNA damage was detected using a red fluorescent antibody (Alexa Fluor 555) against phosphorylated H2AX. At the same time, cell viability was investigated by Image-iT DEAD Green, which permeates when the plasma membrane is compromised. HEKa cells were treated for 5 min with UV irradiation and subsequently cultured under normal conditions for one day. The results show HEKa cells suffering this treatment had dramatically increased DNA damage (red) and cell death (green) seen simultaneously. By contrast, after incubating with MelNPs for 3 days, HEKa cells with the same 5 min UV irradiation and subsequent 24 hour incubation displayed no DNA damage and excellent viability [Figure 14a, Figure 14b,].

(PECASE) Biomolecular Programming of Discrete Nanomaterials for Sensors, Templates and Mimics of

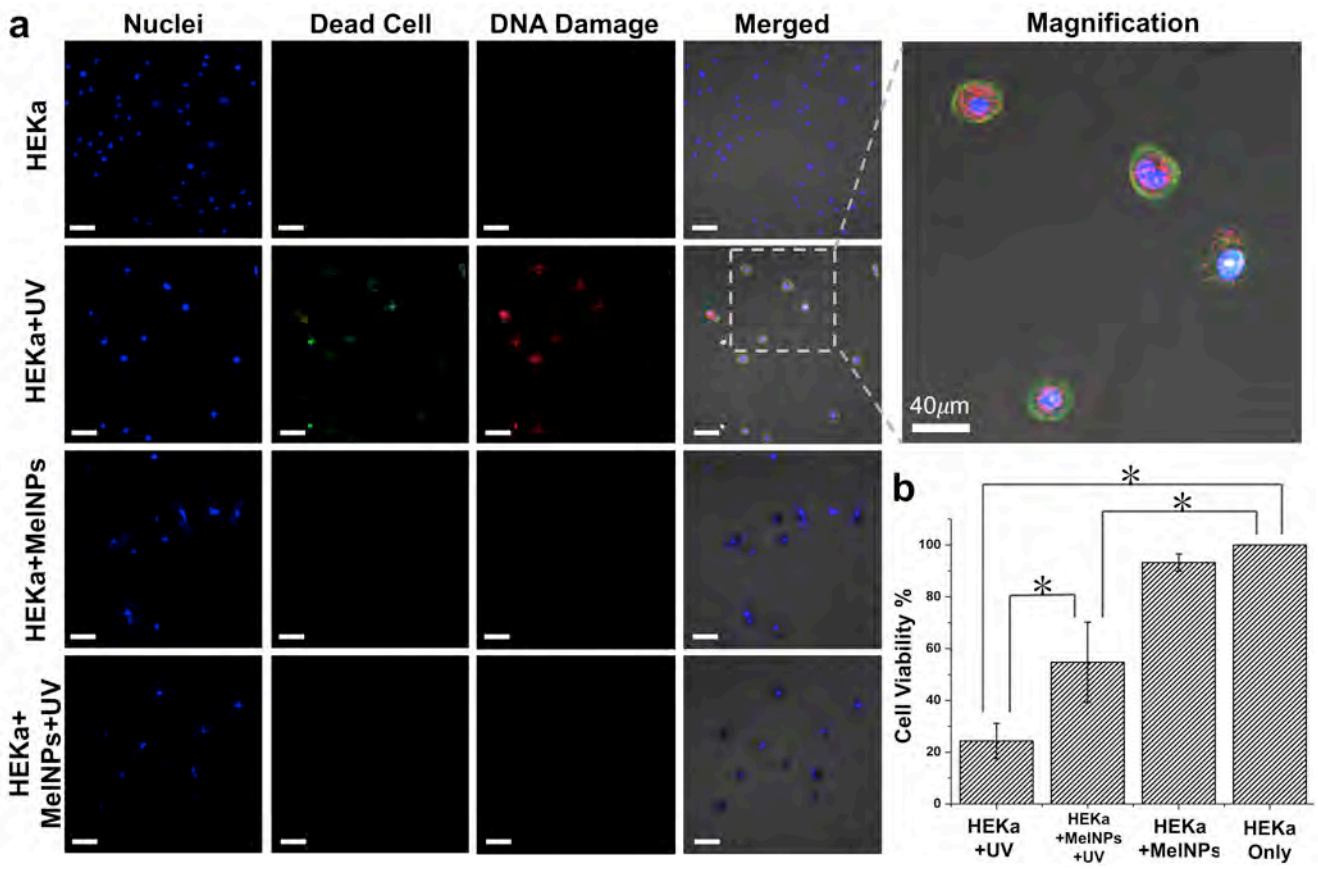

Figure 14. Evaluation of MelNPs as protective materials against UV damage to keratinocytes. a) DNA damage evaluated by light microscopy for HEKa cells with/without incubation with MelNPs and HEKa cells. Nuclei were stained by Hochest 33342 and indicated as blue; Cell membranes were stained by Image-iT DEAD Green and showed as green. b) Crystal violet assay for HEKa cell viability with/without UV or/and MelNP treatment. Scale bars are 80 μm.

In conclusion, we have worked towards being able to prepare, in a facile manner, melanin-like nanoparticles (MelNPs) by spontaneous oxidation of dopamine in alkaline solution. MelNPs were taken up by HEKa cells followed by accumulation as prenuclear caps, in an uneven pattern. This cellular distribution is similar to that observed for natural melanosomes occurring in natural human skin *in vivo*, observed in tissue culture of keratinocytes treated with extracted melanosomes, and in co-cultures of melanocytes with keratinocytes. Assays indicate that MelNPs are transported by similar pathways as natural melanosomes with subsequent degradation of MelNPs observed in HEKa cells after incubating for 3 days to generate structures observed in natural systems. Finally, the UV photoprotective qualities of synthetic MelNPs was demonstrated. Considering limitations in the treatment of melanin-defective related diseases and the biocompatibility of these synthetic MelNPs, these systems have potential as artificial melanosomes in the development of novel therapies for supplementing the biological functions of natural melanins. We note, that of particular relevance to DOD, is the extraordinary capability of these materials to perform as protective systems for cells and tissues. It is known for example that toxins, as well as gamma and UV-light are absorbed by melanin-

like materials. We imagine that translation of these materials to protective skin coatings, may benefit the war fighter. It should also be noted that we view this as part of an ongoing effort to elucidate the basic properties of these kind of materials related to key areas: 1) Magnetism, 2) Structural color, 3) Toxin and radiation absorption.

A Study of the Basic Physical Properties of Synthetic Melanin and in Particular the Iron Coordination Chemistry that Defines these Structures – Manuscript in Review

In this review period we have developed a synthetic method for increasing and controlling the iron loading of synthetic melanin nanoparticles and use the resulting materials to perform a systematic quantitative investigation of the structure-property relationship of synthetic melanin. A comprehensive analysis by magnetometry, electron paramagnetic resonance (EPR), and nuclear magnetic relaxation dispersion (NMRD) reveals the complexities of the magnetic behavior and how these intraparticle magnetic interactions manifest in useful material properties such as their performance as MRI contrast agents. This analysis allows predictions of the optimal iron loading through a quantitative modeling of antiferromagnetic coupling that arises from proximal iron ions. These studies provide a detailed understanding of this complex class of synthetic materials and gives insight into interactions and structures prevalent in naturally occurring melanins.

The natural function and structure inherent to the biomaterial melanin has sparked interest in its utility across a broad range of biomedical applications.(43) Recent work has shown that through the self-oxidation polymerization of dopamine under alkaline conditions, synthetic mimics of natural melanin, with similar chemical structure as well as physical and biological properties, can be achieved.(44, 45) These polydopamine (PDA)-based synthetic nanoparticles retain many of the desirable properties of natural melanin and have been studied for use in catalysis,(46) free radical quenching,(44, 45) inkjet printing,(47, 48) photothermal therapy,(49, 50) and structural coloration.(51, 52) Many of these applications rely on the strong binding affinity of catechol-based functional groups, allowing robust coordination of various transition metals.(53-55) Despite the proliferation of work in this area, the complex, amorphous nature of the material necessitates a multi-technique approach to elucidate their physical, electronic, and magnetic structures.(45) We have employed a host of complementary techniques to define the properties of synthetic melanin nanoparticles (SMNPs) prepared by a new synthetic route that, critically, provides tunability of the Fe(III) content. This synthetic route leads to particles that incorporate high concentrations of high-spin Fe(III), and therefore, our study includes an investigation of their ability to act as magnetic resonance imaging (MRI) contrast agents.

Synthetic melanin-based materials are of particular interest as MRI contrast agents due to their excellent biocompatibility and ability to coordinate isolated paramagnetic metal centers.(56, 57) The catechol functionalized network of the nanoparticle acts as a scaffold for chelation of paramagnetic metal ions, leading to T_1-weighted MRI contrast. Although a number of studies have been published on such materials, questions remain about the origin and the path to optimization of the MRI contrast.(45) Our approach initially involved the development of synthetic methods to achieve high

metal loadings, as T_1-weighted MRI contrast should scale linearly with the number of isolated paramagnetic centers. The obvious method for preparation of SMNP MRI contrast agents is to expose the already-formed SMNP to a solution containing Fe(III) cations; an approach we term, the post-synthetic strategy (Figure S1). The post-synthetic strategy is convenient and allows for the complexation of a variety of cations.[24] However, this approach generally limits the metal loading efficiency, which in our hands results in less than 1% iron by mass.(56) Although this situation can be improved somewhat by decreasing the surface-to-volume ratio of SMNP,(56) achieving ultrahigh Fe(III) loadings (i.e. > 5%) for optimizing and studying the magnetic properties and resulting SMNP-based MRI contrast, has remained elusive.

Another important question is how water relaxation can occur in a system with strongly chelating catechol units interacting with Fe(III). Considerable insight into the coordination environment of catechol-based materials in general has been gained through electron paramagnetic resonance (EPR) and Mössbauer spectroscopies.(58-62) EPR in particular has given a wealth of data regarding the presence or absence of radical electrons and trace metal ions. However, systems with higher quantities of Fe(III) are difficult to analyze by these techniques due to non-uniform coordination environments and inter-ion magnetic interactions. By contrast, magnetometry excels at the analysis of higher magnetic concentrations and can also reveal details of the local anisotropy and coupling interactions that are vital to understanding the magnetic nature of highly doped materials. Notably, although a variety of analytical methods have been individually employed in characterizing natural melanins,(63-65) a thorough analysis by combined methods allows us to exploit the specific strengths of each technique to understand the coordination environment and magnetic interactions of synthetic mimics of melanin, and in the future, potentially the natural biomaterial itself in all its various forms.

Synthesis and Characterization of SMNPs by Electron Microscopy. To prepare a series of SMNP contrast agents with a broad range of Fe(III) loadings for systematic structure-property relationship analysis, the development of a general Fe(III)-doping strategy to achieve > 5% loading was required. This was accomplished through the use of a pre-polymerization chelation strategy, which employs a mixture of Fe(III)(dopamine)$_3$(66) and free dopamine as the precursors for the formation of Fe(III)-chelated SMNPs (Scheme 1). During the polymerization process, under alkaline conditions, Fe(III) can be continuously incorporated into the SMNP as it forms, allowing tunable, high doping levels of metal ions inside the particle. We have employed this pre-polymerization doping strategy (SMNP-*i* (*i*=2-5)) and the standard post-polymerization doping strategy (SMNP-1) to synthesize a series of Fe(III)-doped SMNPs with various Fe(III) concentrations. For example, Fe(III) loading in SMNP-5 is 10.26%, which approaches the maximum theoretical loading of 10.7% if one assumes that one Fe(III) ion is coordinated to three catechol units. Additionally, our pre-doping one-pot strategy features several advantages over the post-synthetic strategy including efficiency of synthesis, leading to generally higher yield reactions due to less purification work.

Scheme 1. Preparation of SMNP-*i* (*i*=0-5) samples: (a) Post-synthetic strategy for SMNP-1, (b) Pre-polymerization doping strategy for SMNP-2, SMNP-3, SMNP-4, and SMNP-5, and (c) SMNP-*i* (*i*=0-5) samples with different Fe(III) concentrations

(PECASE) Biomolecular Programming of Discrete Nanomaterials for Sensors, Templates and Mimics of

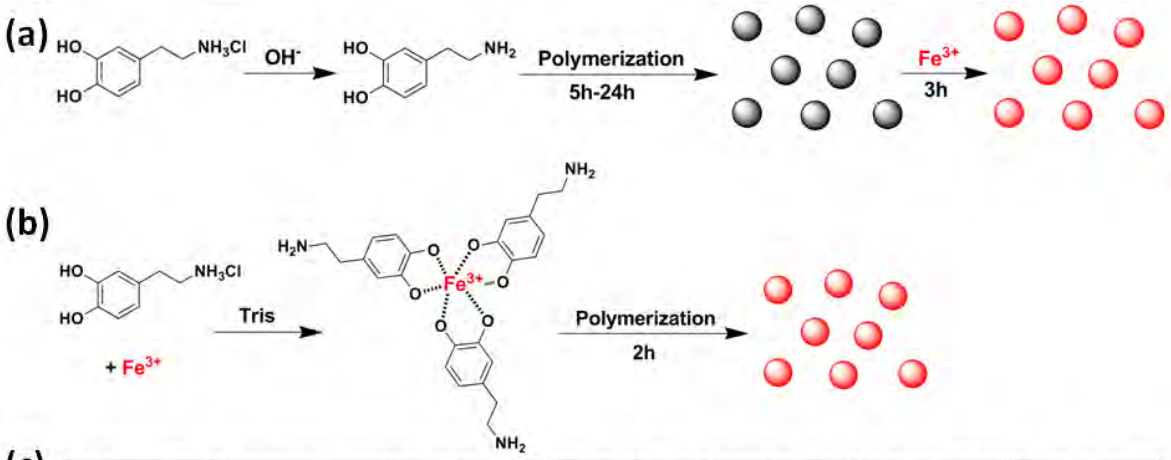

(c)

Sample	SMNP-0	SMNP-1	SMNP-2	SMNP-3	SMNP-4	SMNP-5
Fe(III)%	0	0.46	1.89	2.88	5.86	10.26
Method	-	a	b	b	b	b

All SMNPs are characterized by transmission electron microscopy (TEM) and scanning electron microscopy (SEM) to quantify their size and uniformity. The combination of TEM, cryo-TEM and SEM (Figure 15) shows spherical nanoparticles with diameters in the range of 140 to 250 nm. The presence of metal inside the nanoparticles was evident in the high contrast they exhibit when observed via high angle annular dark field (HAADF)-STEM and bright field scanning transmission electron microscopy (BF-STEM). Selected area HAADF-STEM coupled with energy dispersive X-ray spectroscopy (EDS) further confirm the presence of Fe(III) ions localized in the nanoparticles. The EDS profiles suggest that the content of iron in the testing areas of SMNP-4 were significantly higher than that on the grid surface background, which is in good agreement with the elemental mapping analysis results (Figure 15). Together, these results strongly suggest that SMNP-*i* (*i*=0-5) are morphologically similar at the nanoscale and hence, we expect them to differ only in the average number of unpaired spins imparted by the Fe(III) iron content.

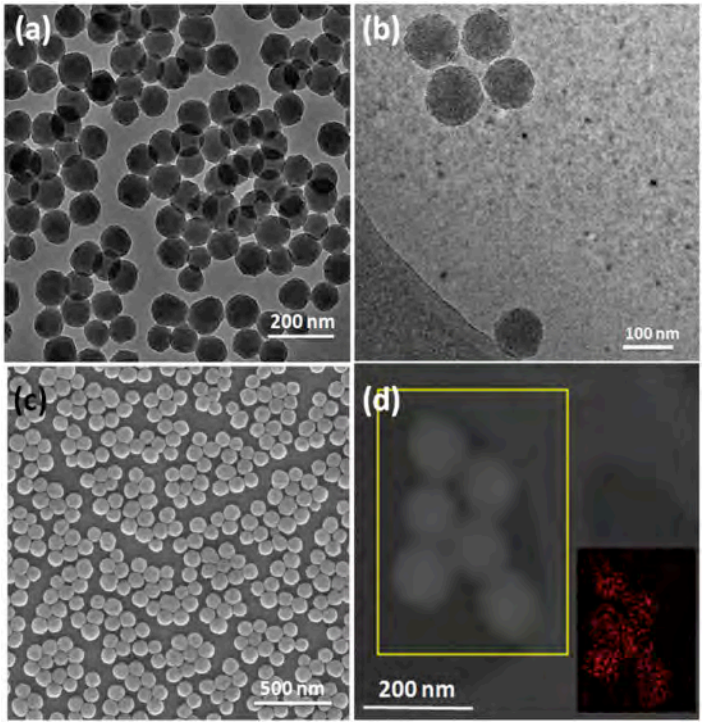

Figure 15. Representative electron microscopy characterization of SMNP-4: (a) TEM; (b) cryo-TEM; (c) SEM; and (d) HAADF-STEM (insert is the selected area EDS Fe elemental mapping image).

Characterization of SMNPs by NMRD and MR Imaging Analysis. Additional unpaired spins present in the higher Fe(III)-loaded samples should have a strong effect on the relaxometry of proximal solvent protons. This effect, the source of T_1 contrast enhanced MRI, was probed through measurement of the longitudinal water proton relaxation rates (R_1) as a function of applied magnetic field for all SMNP samples. ^{1}H Nuclear Magnetic Relaxation Dispersion (NMRD), allows an accurate determination of the field dependence of R_1 that arises from the magnetic interaction between the metal centers and the solvent.[67, 68] This takes place either through chemical exchange between the bound water and the bulk water molecules (*inner sphere*), or through a long-distance interaction with outer sphere water molecules that rapidly diffuse near the paramagnetic centers (*outer sphere*). Shown in Figure 16 are the ^{1}H NMRD profiles of SMNP-*i* (*i*=1-5) measured at 298 K in the range 2.3 mT to 1.6 T. The data are expressed in terms of relaxivity, r_{1p}, which is defined as the relaxation rate enhancement induced by 1 mmol/L of paramagnetic ion. With the exception of the lowest Fe(III)-loading sample, the NMRD profiles of the SMNPs show a similar shape characterized by a low field plateau (ca. 0.1-1 MHz), followed by a dispersion around ≈ 2-4 MHz and a relatively small increase at frequencies above ca. 30 MHz. The single dispersion displayed at about 3 MHz corresponds to a correlation time $t_C \approx 9\times10^{-11}$ s. Due to the slow rotational dynamics (long t_R values) of paramagnetic centers in these nanoparticles, we attribute this correlation time to the electronic relaxation time t_S, which has been reported to fall in the range 10^{-11} s to 10^{-9} s.[69] The clear increase of r_{1p} above *ca*. 30 MHz makes it evident that: (1) t_S is field dependent; and (2) t_S represents a predominant factor in the determination of t_C. This behavior resembles that reported by Bertini *et al.* in the case of the ^{1}H NMRD profiles of Fe(III) aqua ions in different glycerol-water mixtures.[70] By increasing the viscosity, the relative

contribution of t_R to t_C with respect to t_S decreases and the relaxivity in the high field region increases. The NMRD profile of the iron-binding glycoprotein transferrin shows a similar general trend, although with a more pronounced decrease of r_{1p} with frequency in analogy with that observed for SMNP-1.(71) All these features suggest the presence of one or more water molecules bound to the metal centers (q≥1), at least for a certain population of the Fe(III) centers.

The shape and amplitude of the NMRD profiles suggests various contributions to the relaxivity. The relative complexity of the shape of the profiles reflects the distribution of different populations of species with different coordination environments and thus magnetic properties. The outer sphere contribution to relaxivity, predominant in the case of *tris*-catechol-Fe(III) species (q=0), is generally rather small and can be estimated at approximately 1-2 mM^{-1} s^{-1}.(72) When water is bound to an Fe(III) cation in a macromolecule, the long exchange lifetime often represents a limiting effect on relaxivity. However, as shown by the case of fluoromethemoglobin,(73) high relaxivity values can be associated with fast exchanging water molecules H-bonded to hydroxide ligands on or next to Fe(III) ions (*second sphere* contribution).(73) The dominant role of this mechanism has recently been discussed in the case of polycatechol nanoparticles.(74) All these contributions, with different weights, are likely to play a role in determining the relaxation behavior of these SMNPs.

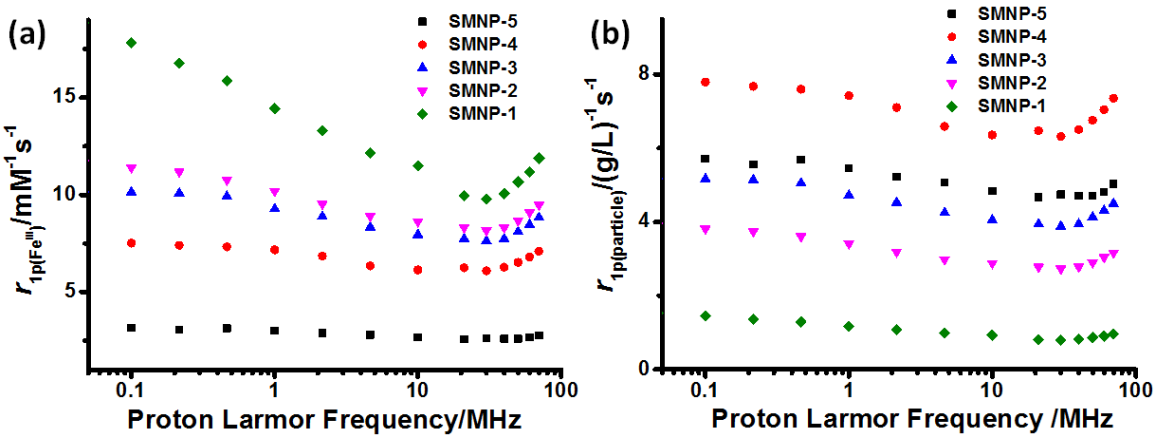

Figure 16. (a) ^{1}H NMRD profiles for SMNP-*i* (*i*=1-5). The x-axis is proton Larmor frequency, y-axis is r_{1p} value per Fe(III) ion ($r_{1p(Fe(III))}$) for each SMNP. (b)^{1}H NMRD profiles for SMNP-*i* (*i*=1-5). The x-axis is proton Larmor frequency, y-axis is r_{1p} value per SMNP ($r_{1p(particle)}$).

Since each SMNP can contain many chelated Fe(III) ions, it is interesting to consider the per particle-relaxivity ($r_{1p(particle)}$) to describe the local concentration necessary to achieve the desirable T_1 MR imaging contrast under different magnetic fields.(75) Figure 16b shows the calculated $r_{1p(particle)}$ of each SMNP. Interestingly, the plots of $r_{1p(particle)}$ and $r_{1p(Fe(III))}$ show different trends. Whereas $r_{1p(Fe(III))}$ reveals a diminishing return for additional Fe(III), the plot of $r_{1p(particle)}$ shows there is an upper limiting doping level (i.e. SMNP-4) after which the ^{1}H NMRD shows a decrease in relaxivity over all frequencies. These data lead to the counterintuitive result that highly paramagnetically-doped particles are inferior to those doped with lower levels of Fe(III) ions.

Magnetochemical analysis of SMNP. Several intriguing questions are suggested by the relaxivity data: (1) Is the T_1 contrast arising from an inner-sphere binding event, despite the propensity for catechol to form strong *tris*-chelates in neutral and basic solutions? (2) Why is there not a linear increase in the relaxivity response with additional Fe(III) cations, as would be expected for T_1 contrast? To address these questions directly, we turned to techniques that are sensitive to the local spin states as well as the ensemble properties of the magnetic structure.

EPR spectra of frozen solutions were collected at 125 K (in collaboration with Dr. Eric Walter, PNNL - Figure 17). The characteristic spectrum of the persistent radical, that is a hallmark of all melanins, is visible in samples with less than 2% iron. As reported, paramagnetic metals can reduce the amplitude of this peak,(76) completely suppressing it at high loadings. All iron-containing samples show a peak at 1600 G (g=4.3) which is attributed to high spin Fe(III) in sites of low symmetry of tetrahedral or octahedral coordination.(64) The width of this peak increases with increased iron loading due to spin-spin dipolar coupling.(77) From these data, we determined the change in the full width at half maximum as a function of total iron, with the linear progression suggesting that the iron loading is evenly distributed in a 3-D matrix of sites, as opposed to either lower dimensional arrangements or clusters (Figure S8).(78)

At the highest iron loading levels, a very broad spectrum centered near g=2 is evident. In many systems, a spectrum of this form is due to superparamagnetic or ferromagnetic particles. Therefore, the spectrum of SMNP-5 was recorded over a wide range of temperatures to explore the magnetic properties of this species (Figure 17b).(79) However, unlike a ferromagnetic material, which would have a constant intensity, or a superparamagnetic material that would have spectra that would broaden and shift to lower field as the temperature is lowered, the spectra increase in amplitude as the temperature is lowered to 20 K, but then sharply diminish in amplitude at 3.5 K. This behavior indicates the occurrence of a more complex magnetic behavior that gains in strength with increasing Fe(III) loading.

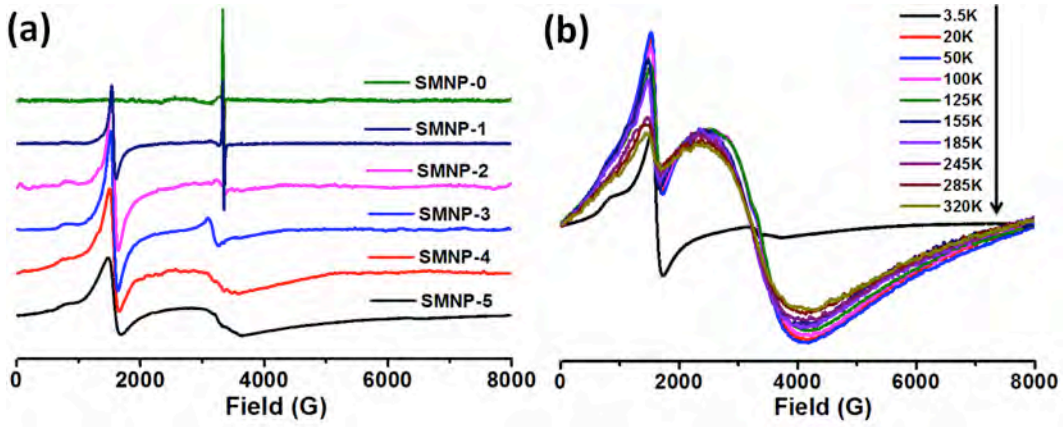

Figure 17. (a) Experimental EPR spectra of SMNP-*i* (*i*=0-5). (b) Temperature-dependent EPR analysis of SMNP-5.

To elucidate the origin of this alteration in the magnetic structure at high Fe(III) cation concentrations, the temperature dependence of the SMNP magnetic susceptibility was investigated by Superconducting Quantum Interference Device (SQUID) magnetometry (Figure 18a). The lowest Fe-loading sample (SMNP-1) was expected to largely exhibit characteristics of the isolated octahedral high-spin d^5 configuration of Fe(III) (S=5/2) as demonstrated by the EPR data. Indeed, the product of magnetic susceptibility and temperature per mole Fe ($\chi_M T$) at 300 K approaches the expected spin-only value of 4.375 emu K cm^{-3} mol^{-1} for a purely Fe(III)-containing sample. This close agreement precludes the possibility of significant Fe(II) and low-spin Fe(III) populations, as they would lead to significant alterations in the $\chi_M T$ value. As temperature is decreased from 300 K, the effects of antiferromagnetic Fe(III)-Fe(III) interactions begin to manifest in the $\chi_M T$ data. For SMNP-1 with only 0.46% Fe(III) loading, the majority of Fe(III) centers are sufficiently isolated so as to display their full, uncoupled moment. However, a non-negligible subset of Fe(III) are close to other Fe(III) sites and thus display antiferromagnetic interactions that lower the overall $\chi_M T$ value. As we increase the Fe(III) concentration up to 10.26% (SMNP-5), deviations from the spin-only expectation become more drastic, leading to a drop of more than 20% in the $\chi_M T$ product at room temperature.

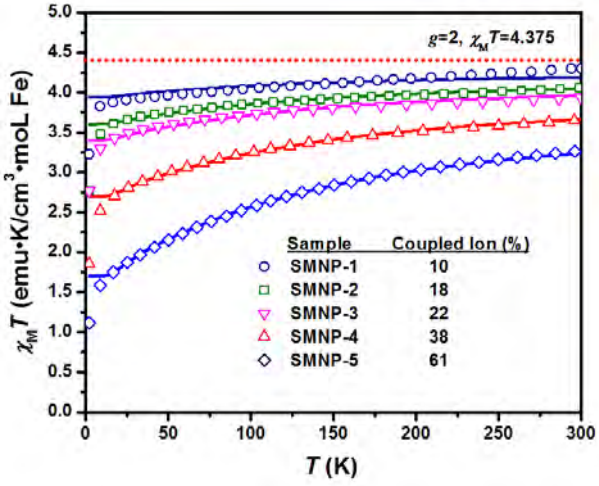

Figure 18. (a) Temperature dependence of the product of magnetic susceptibility and temperature ($\chi_M T$) for SMNP-*i* (*i*=1-5). The dotted line describes the behavior of an isolated, isotropic Fe(III) ion. Solid lines represent a global fit of the data between 25 and 300 K as described in the text.

We find that a relatively simple model, incorporating an isotropic *g* value and magnetic coupling constant ($J_{\mathrm{Fe-Fe}}$) is able to satisfactorily explain the coupling behavior of Fe(III). In this model, we need only consider two general types of Fe(III) centers: magnetically isolated Fe(III), and magnetically coupled Fe(III). This assumption is based on the weak superexchange pathway that the catechol functional groups of PDA provides. Indeed, model molecular Fe(III) catecholate dinuclear complexes display coupling constants of less than 30 cm^{-1}, even when only separated by a single catecholate oxygen.(80-82) The ratio between the uncoupled and coupled Fe(III) subsets is fitted along with an isotropic *g* and $J_{\mathrm{Fe-Fe}}$ value by simultaneous global fitting of all susceptibility data. Uncoupled Fe(III) is modeled as an ideal paramagnetic S=5/2 Fe(III), whereas coupled Fe(III) is modeled through an HDVV Hamiltonian (Eq. 1) where $\widehat{\boldsymbol{S}}_1$ and $\widehat{\boldsymbol{S}}_2$ are spin operators for equivalent interacting spins.

Although most natural and synthetic melanin systems have been shown to possess some radical electron character,(45, 83, 84) we do not find it necessary to include radical electrons in our model. This is corroborated by measuring magnetic susceptibility of equivalently-synthesized pure melanin nanoparticles (SMNP-0) without Fe(III) loading which shows negligible paramagnetic moment across all temperatures (Figure S9). This does not imply that no radical population is present, only that it is necessarily low enough to be inconsequential to the overall magnetism. In fact, EPR spectra (Figure 17) confirm the presence of organic radicals in SMNP-0 and SMNP-1.

$$\hat{\mathrm{H}} = -2\mathrm{J}_{\mathrm{Fe-Fe}}\,\hat{\mathrm{S}}_1 \bullet \hat{\mathrm{S}}_2 \qquad (1)$$

The fitting results reveal antiferromagnetic coupling (g=2.05±0.04; $J_{\mathrm{Fe-Fe}}$=−24.8±2.7 cm^{-1}) that corresponds well to molecular Fe-catechol systems.(80, 85, 86) Of particular note is that at very high Fe(III) loadings (SMNP-5), over half of the Fe(III) is now involved in magnetic coupling interactions, leading to a significant drop in the moment even under ambient temperature conditions. This behavior tracks well with the low $r_{1p(Fe(III))}$ of SMNP-5 sample. From the view of MRI contrast agents, this antiferromagnetic coupling tempers the advantage of high loading because of the significant reduction in room temperature moment per iron center compared with less concentrated Fe(III) samples. Additionally, the magnetically coupled Fe(III)–Fe(III) interactions can alter the nature of the relaxation, shifting the SMNP towards T_2-weighted agents at high concentrations. These factors indicate that there will be an optimal Fe(III) concentration. This relatively strong coupling also indicates that short Fe(III)–Fe(III) ligand-based bridges can exist within the PDA structure, an intriguing result considering that mononuclear molecular Fe(III)-catechol exists as a mixture of bis- and tris-catechol-Fe(III) species at our synthetic conditions (pH ~9).(87) Since a tris-catechol binding mode would inhibit the formation of effective superexchange bridges, the strength of coupling we observe may indicate a low catechol coordination number for Fe(III) within the SMNP. If, in fact, the PDA structure is limiting the catechol coordination, this opens the exciting possibility that water is able to directly bind to Fe(III) centers or interact with hydroxides directly bound to Fe(III) centers, thus explaining the strong MRI contrast observed for Fe(III)-coordinated synthetic melanin.(56)

Further evidence of limited Fe-catechol bonding was obtained by scrutinizing the deviations from ideal paramagnetic behavior observed at very low temperature. These deviations are caused by magnetic anisotropy induced by a low-symmetry coordination environment as well as Zeeman splitting due to the applied field. To isolate the effects of the magnetic anisotropy we performed a series of low temperature, variable field measurements for SMNP-1, which has the lowest amount of coupled Fe(III) (Figure 18a). We focus on SMNP-1 because 90% of the Fe(III) is in the uncoupled state, and the magnetic influence of the remaining 10% is minimized due to its relative isolation in the antiferromagnetically coupled (S=0) state at low temperature. Under these approximations, the molar magnetization values in Figure 18a are solely due to uncoupled Fe(III) ions. By fitting to an axially anisotropic Hamiltonian (Eq. 2) using the MagProp module of DAVE 2.3 (Figure 19),(88) a small but non-negligible axial anisotropy is determined to be present (D=0.88±0.29). Interestingly, this value corresponds to that observed for mono-catechol-bound Fe(III) in acidic aqueous solution (D=0.82),

but is significantly higher than the bis- and tris-catechol-bound Fe (III) (*D*=0.42 and *D*=0.32, respectively).(60) High Fe(III) concentration samples (SMNP-2 through SMNP-5) gave similar results although with less satisfactory error values due to the added complication of large contributions from coupled Fe(III).

$$\hat{H} = g\mu_B \hat{S} \cdot B + D[\hat{S}_z^2 - \frac{S(S+1)}{3}] \quad (2)$$

The magnetic evidence strongly suggests that despite the high concentration of catechol in SMNP materials and pH values during synthesis that should initially favor a tris-catechol binding mode, Fe(III) is largely coordinated as the mono-catechol in the final product. As this result was somewhat counterintuitive, UV-vis spectroscopy was employed to corroborate our magnetic analysis. Figure 19b shows that both high (SMNP-5) and low (SMNP-3) Fe(III) loadings exhibit a broad peak at 710 nm, which is indicative of mono-catechol-Fe(III) complexes.(59, 87, 89) In stark contrast to previously-studied free Fe(III) catechol systems,(87, 89) this peak persists, even at very basic pH values for 24 h with no indication of bis- or tris-catechol formation. These data suggest that melanin-based MRI contrast agents may allow for water exchange through an “inner-sphere” T_1 relaxation, even for Fe(III) embedded within the nanoparticle.(56, 90)

From the combination of magnetometry and magnetic spectroscopy (EPR) we can conclude that isolated paramagnetic iron centers exist throughout the SMNPs. At higher concentrations, the Fe(III) does not form oxide particles that would show ordered magnetic behavior but does form weak antiferromagnetic superexchange interactions that effectively cancel out a significant portion of the 300 K magnetization. Additionally, the high magnetic anisotropy indicates a low-symmetry environment that is not consistent with tris-catechol coordination of Fe(III); thus the superexchange is likely mediated by diamagnetic bridging ligands and not the polymer backbone.

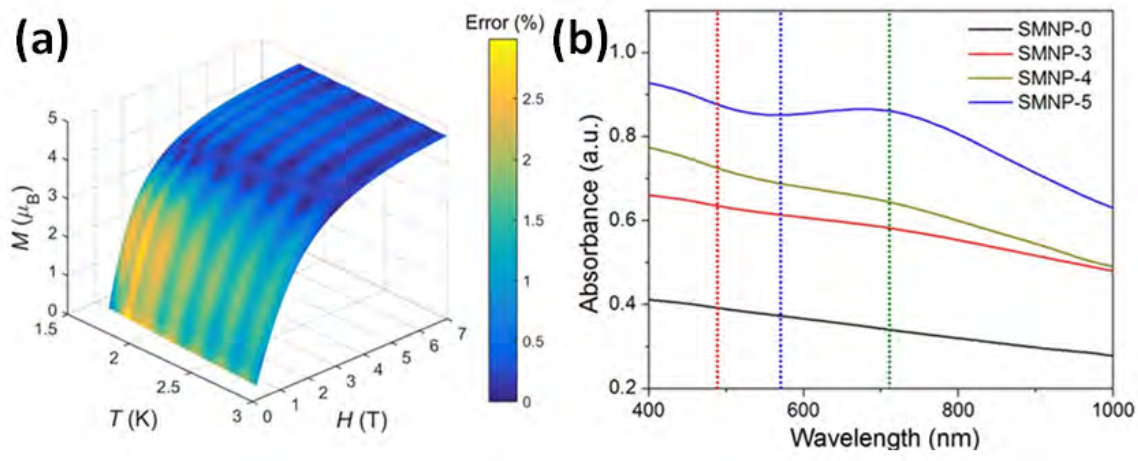

Figure 19. (a) Plot of variable-temperature variable-field magnetization data for SMNP-1. The color bar represents the difference between experimental data and fitting results. A standard 2D *M* vs. *H*/*T* plot is shown in Figure S10. (b) UV-vis spectra of 0.1 mg/mL SMNP showing the transition from a featureless absorption for SMNP-0 to a well-defined yet broad structure in SMNP-5. Absorption peaks for mono-(~710 nm), bis-(~570 nm), and tris-catechol (~490 nm) are identified by dashed green, blue, and red, lines, respectively.

In summary, a new technique for accessing SMNPs with tunable iron loadings has opened the door for their magneto-structural analysis through the combined utilization of SQUID magnetometry, EPR and ^{1}H $1/T_1$ NMRD. The results presented in this report also suggest a number of avenues for optimizing MRI contrast in synthetic melanin nanoparticles: (1) Because high Fe(III) loading leads to a lowering of the moment per Fe(III) center, decreasing coupling between paramagnetic centers would necessarily increase the magnetic moment at higher loadings. This, in turn, could increase the T_1 relaxation rate of surrounding water protons due to the presence of more unpaired electron spins. This could be achieved by a number of synthetic approaches including the expansion of the polymer backbone to increase the distance between Fe(III) binding sites or incorporating higher-spin, weaker-coupling ions. (2) Alternatively, the antiferromagnetic coupling could be disrupted through the creation of an alternate, small-spin magnetic coupling channel between Fe(III) and an organic radical electron or S=1/2 transition metal centers such as Cu(II). Thus antiferromagnetic coupling would result in a net S=2 state even at very high ion loadings, preventing the decrease of magnetic moment. Particles of this type would, however, likely exhibit T_2-weighted contrast similar to other highly coupled particle systems such as magnetite. (3) Since mono-catechol coordination is likely the result of steric hindrance created by the rigid cross-linked polymer backbone, modulating this steric hindrance may create better intra-particle channels for replacing water at Fe(III) binding sites while still preventing multi-catechol binding. Alternatively, the polymer backbone can be modified to electronically enhance the local water exchange rate at Fe(III) sites.

With the current interest in metal-doped melanin and polycatechol-based nanomaterials, a fundamental understanding of the electronic and magnetic structure is vital. The conclusions from these initial studies in this area offer potential synthetic targets that could lead to more directed syntheses of effective contrast agents. More broadly, these combined characterization tools should provide insight into natural melanins and therefore, any potential differences or similarities between their various forms, and their synthetically accessible mimics.

Summary and DOD Relevance

We have worked on the development of biomolecule-polymer conjugates as responsive elements for assembly of complex morphology switchable nanomaterials, and have combined this with an effort in nature-inspired materials with a particular focus on synthetic, or artificial polymeric organelles, including melanosomes. Relevance of these projects to the DOD interests include the possibility of employing the resulting materials in advanced biochemical sensors, where recognition elements combined with stability and long term use are needed; hence our interest in stabilized but responsive biomolecular materials and conjugates between 2011 and 2016. In terms of melanin work, we see strong relevance in these bioinspired materials that are capable of acting as structural color elements, with unusually high refractive indices and with an understanding of synthetic processes leading to morphological control. This would lead to an ability to develop materials that have iridescent structural

color, but capable of broad band absorbance, combined with unusual magnetic properties. The fact that very little is known about their natural biosynthesis, and their properties in general, means there is a rich source of chemical information to mine, and potentially utilize in new device applications. Thirdly, we have developed liquid cell TEM (LCTEM) as a means for studying these complex responsive systems. This work has lead to our recent developments of instrumentation allowing the establishment of chemical gradients, and ongoing work to develop variable temperature LCTEM (VT-LCTEM) methodologies for looking at porous materials including covalent organic frameworks. The potential power of this technique is enormous. It would become the third arm in the TEM suite of characterization tools together with cryogenic, and standard high vacuum TEM. We anticipate that the kinds of tools described here for arraying and setting up the reactions is going to be a critical and commonplace tool. This is a tool that was patented, and we are currently pushing the technology to make it fit for inclusion in designs for dedicated liquid cell TEM instruments of the future. This would be the “Vitrobot” (an automated system for setting up cryogenic TEM experiments) of liquid cell TEM, and would allow anyone capable of performing standard TEM experiments to conduct what is now an extremely specialized and challenging imaging technique. Ongoing work will include methods for tracking particles automatically and quantifying their growth and motion in solution. This tool, implemented in real time, will allow the user to immediately assess the quality of the data, and to make decisions on the fly regarding how long to image and at what magnification. In summary, while there are many unsolved problems, they are all solvable, with a tremendous upside potential.

Supported Personnel

Joseph Patterson	(Postdoctoral fellow) - LCTEM
Nia Bell	(Postdoctoral fellow) – Polymeric systems from ROMP
Julia Michaelis	(Postdoctoral fellow) – Biomolecule-polymer conjugates
Matthew Thompson	(Postdoctoral fellow) – General synthetic methodologies
Miao-Ping Chien	(PhD) – Peptide and Nucleic Acid-based Materials
Ti-Hsuan Ku	(PhD) – Peptide-based Materials
Lyndsay Randolph	(PhD) – Peptide-based Materials
Anthony Rush	(PhD) – Nucleic Acid-based Materials
Carrie James	(PhD) – Nucleic Acid-based Materials
Xiujun Yue	(PhD) – Melanin nanoparticles
Nanzhi Zang	(PhD) – Melanin nanoparticles

(PECASE) Biomolecular Programming of Discrete Nanomaterials for Sensors, Templates and Mimics of

Collaborations and Interactions

We have developed liquid cell TEM both at UC San Diego with our own instrumentation, and with collaborators at Pacific Northwest National Laboratories – Dr. Nigel Browning and Dr. James Evans. Additional work includes collaborations with Prof. Chiwoo Park (Florida State) and Prof. Francesco Zerbetto (University of Bologna, Italy).

We have developed Melanin-based systems in collaboration with Prof. Matt Shawkey, Akron and Dr. Eric Walter at PNNL. In addition, we collaborate on magnetic data with Prof. Jeffrey Rinehart at UC San Diego and Prof. Mauro Botta at the University of Piemonte, Italy.

Relevant Publications – 27 in total - (work supported by this grant: 2011-2016)

1) Chien, M. –P.; Thompson, M. P.; Gianneschi, N. C.; "DNA-nanoparticle micelles as supramolecular fluorogenic substrates enabling catalytic signal amplification and detection by DNAzyme probes" *Chem. Comm.,* **2011***, 47*, 167-169
2) Ku, T.-H.; Chien, M.-P.; Thompson, M. P.; Sinkovits, R. S.; Olson, N. H; Baker, T. S.; Gianneschi, N. C. "Controlling and Switching the Morphology of Micellar Nanoparticles with Enzymes" *J. Am. Chem. Soc.* **2011**, *133*, 8392-8395
3) Chien, M. –P.; Gianneschi, N. C. "A Morphology Dependent Bioorganic Template for Inorganic Nanowire Synthesis" *Small*, **2011**, *7*, 2041-2046
4) Hahn, M. E.; Gianneschi, N. C. "Enzyme-Directed Assembly and Manipulation of Organic Nanomaterials." *Chem. Comm.,* **2012**, *47*, 11814-11821
5) Randolph, L. M.; Chien, M. –P.; Gianneschi, N. C. "Biological Stimuli and Biomolecules in the Assembly and Manipulation of Nanoscale Polymeric Particles" *Chem. Sci.* 2012, *3*, 1363-1380
6) Chien, M. –P.; Thompson, M. P.; Lin, E. C.; Gianneschi, N. C. "Fluorogenic Enzyme-Responsive Micellar Nanoparticles" *Chem. Sci.* **2012**, *3*, 2690-2694
7) Chien, M.-P.; Carlini, A. S.; Hu, D.; Barback, C. V.; Rush, A. M.; Hall, D. J.; Orr, G.; Gianneschi, N. C. "Enzyme-Directed Assembly of Nanoparticles in Tumors Monitored by In Vivo Whole Animal and Ex Vivo Super Resolution Fluorescence Imaging" *J. Am. Chem. Soc.* **2013**, *135,* 18710-18713
8) Chien, M. –P.; Thompson, M. P.; Barback, C. V.; Hall, D. J.; Gianneschi, N. C. "Enzyme-Directed Assembly of a Nanoparticle Probe in Tumor Tissue" *Advanced Materials.* **2013**, *25*, 3599-3604.
9) Kammeyer, J. K.; Blum, A. P.; Adamiak, L. Hahn, M. E.; Gianneschi, N. C. "Polymerization of Protecting-Group-Free Peptides via ROMP" *Polymer Chemistry* **2013**, *4*, 3929-3933
10) Rush, A. M.; Thompson, M. P.; Tatro, E. T.; Gianneschi, N. C. "Nuclease-resistant DNA via High Density Packing in Polymeric Micellar Nanoparticle Coronas" *ACS Nano* **2013**, *7*, 1379-1387
11) Hahn, M. E.; Randolph, L. M.; Adamiak, L.; Thompson, M. P.; Gianneschi, N. C. "Polymerization of a Peptide-Based Enzyme Substrate" *Chem. Commun.* **2013**, *49*, 2873-2875
12) Proetto, M. T.; Rush, A. M.; Chien, M. –P.; Abellan Baeza, P.; Patterson, J. P.; Thompson, M. P.; Olson, N. H.; Moore, C. E.; Rehingold, A. L.; Andolina, C.; Millston, J.; Howell, S. B.;

Browning, N D.; Evans, J. E..; Gianneschi, N. C. “Dynamics of Soft Materials Captured by Transmission Electron Microscopy” *J. Am. Chem. Soc.* **2014**, *136,* 1162-1165.

13) Thompson, M. P.; Randolph, L. M.; James, C. R.; Davalos, A. N.; Hahn, M. E. Gianneschi, N. C. “Labeling Polymers and Micellar Nanoparticles via Initiation, Propagation and Termination with ROMP” *Polymer Chemistry* **2014**, *5*, 1954-1964
14) Rush, A. M.; Nelles, D. A.; Blum, A. P.; Barnhill, S. A.; Tatro, E. T.; Yeo, G. W.; Gianneschi, N. C. “Intracellular mRNA Regulation with Self-Assembled Locked Nucleic Acid Polymer Nanoparticles” *J. Am. Chem. Soc.* **2014**, *136*, 7615-7618.
15) James, C. R.; Rush, A. M.; Insley, T.; Vukovic, L.; Kral, P.; Gianneschi, N. C. “Poly(oligonucleotide)” *J. Am. Chem. Soc.* **2014**, 136, 11216-11219.
16) Blum, A. P.; Kammeyer, J. K.; Yin, J.; Crystal, D. T.; Rush, A. M.; Gilson, M. K. Gianneschi, N. C. “Peptides Displayed as High Density Brush Polymers Resist Proteolysis and Retain Bioactivity” *J Am. Chem. Soc.* **2014**, *136*, 15422-15437
17) Ku, T.-H.; Sahu, S.; Kosa, N.; Pham, K. M.; Burkart, M. D.; Gianneschi, N. C. Tapping a Bacterial Enzymatic Pathway for the Preparation and Manipulation of Synthetic Nanomaterials. *J. Am. Chem. Soc.* **2014**, *136*, 17378-17381
18) Blum, A.P.; Kammeyer, J.K.; Rush, A.M.; Callmann, C.E.; Hahn, M.E.; Gianneschi N. C. Stimuli-Responsive Nanomaterials for Biomedical Applications. *J. Am. Chem. Soc.* **2014**, *137*, 2140-2154
19) Bell, N. C.; Doyle, S. J; Battistelli, G.; LeGuyader, C. L. M.; Thompson, M. P.; Poe, A. M; Rheingold, A.; Moore, C.; Montalti, M.; Thayumanavan, S.; Tauber, M. J; Gianneschi, N. C. “Dye Encapsulation in Polynorbornene Micelles” *Langmuir* **2015**, *31*, 9707-9717.
20) Barnhill, S. A.; Bell, N. C.; Patterson, J. P.; Olds, D. P.; Gianneschi, N. C. Phase Diagrams of Polynorbornene Amphiphilic Block Copolymers in Solution. *Macromolecules* **2015**, *48*, 1152-1161
21) Xiao, M.; Li, Y.; Allen, M.; Deheyn, D.; Yue, X.; Zhao, J.; Gianneschi, N. C. Shawkey, M.; Dhinojwala, A. Bioinspired Structural Colors Produced via Self-Assembly of Synthetic Melanin Nanoparticles. *ACS Nano*, **2015**, *9*, 5454-5460.
22) Patterson, J. P.; Abellan, P.; Denny, M. S.; Park, C.; Browning, N. D.; Cohen, S. M.; Evans, J. E.; Gianneschi, N. C. “Observing the Growth of Metal-Organic Frameworks by In Situ Liquid Cell TEM” *J. Am. Chem. Soc.* **2015**, *137*, 7322-7328.
23) Ma, C. D.; Adamiak, L.; Miller, D. S.; Wang, X.; Gianneschi, N. C.; Abbott, N. L. “Liquid Crystal Interfaces Programmed with Enzyme-Responsive Polymers and Surfactants” *Small* **2015**, 11, 5747-5751.
24) Blum, A. P.; Kammeyer, J. K.; Gianneschi, N. C. “Activating Peptides for Cellular Uptake via Polymerization into High Density Brushes” *Chemical Science* **2016**, *7*, 989-994.
25) Patterson, J. P.; Parent, L. R.; Cantlon, J.; Eickhoff, H.; Bared, G.; Evans, J. E.; Gianneschi, N. C. “Picoliter Drop-On-Demand Dispensing for Multiplex Liquid Cell TEM” *Microscopy and Microanalysis* **2016**, *22*, 507-514.
26) Carlini, A. S.; Adamiak, L.; Gianneschi, N. C. “Biosynthetic Polymers as Functional Materials” *Macromolecules* **2016**, *49*, 4379-4394.

(PECASE) Biomolecular Programming of Discrete Nanomaterials for Sensors, Templates and Mimics of

27) Xiao, M.; Li, Y.; Zhao, J.; Wang, Z.; Gao, M.; Gianneschi, N. C.; Dhinojwala, A.; Shawkey, M. D. "Stimuli-Responsive Structurally Colored Films from Bioinspired Synthetic Melanin Nanoparticles" *Chemistry of Materials* **2016**, *28*, 5516-5521

Patents

2012-207: New Methods for Arranging and Packaging Nucleic Acids for Unusual Resistance to Nucleases and Targeted Delivery for Gene Therapy
http://techtransfer.universityofcalifornia.edu/NCD/23489.html

2015-015: Polymerizing Nucleic Acids
http://techtransfer.universityofcalifornia.edu/NCD/24367.html

2015-036: Displaying Peptides as High Density Brush Polymers Ensures Bioactivity, Proteolytic Resistance, and Cellular Uptake
http://techtransfer.universityofcalifornia.edu/NCD/24556.html

2016-328: Polydopamine-based artificial melanins as intracellular UV-shield

2016-026: Low volume drop dispensing liquid cell electron microscopy sample preparation

References

1. Doherty GJ, McMahon HT. Mechanisms of Endocytosis. Annual Review of Biochemistry. 2009;78(1):857-902. doi: doi:10.1146/annurev.biochem.78.081307.110540. PubMed PMID: 19317650.
2. Zidovetzki R, Levitan I. Use of cyclodextrins to manipulate plasma membrane cholesterol content: evidence, misconceptions and control strategies. Biochimica et biophysica acta. 2007;1768(6):1311-24. doi: 10.1016/j.bbamem.2007.03.026. PubMed PMID: 17493580; PubMed Central PMCID: PMC1948080.
3. Craik DJ, Fairlie DP, Liras S, Price D. The future of peptide-based drugs. Chemical biology & drug design. 2013;81(1):136-47. doi: 10.1111/cbdd.12055. PubMed PMID: 23253135.
4. Kaspar AA, Reichert JM. Future directions for peptide therapeutics development. Drug discovery today. 2013;18(17-18):807-17. doi: 10.1016/j.drudis.2013.05.011. PubMed PMID: 23726889.
5. McGregor DP. Discovering and improving novel peptide therapeutics. Current opinion in pharmacology. 2008;8(5):616-9. doi: 10.1016/j.coph.2008.06.002. PubMed PMID: 18602024.
6. Vlieghe P, Lisowski V, Martinez J, Khrestchatisky M. Synthetic therapeutic peptides: science and market. Drug discovery today. 2010;15(1-2):40-56. doi: 10.1016/j.drudis.2009.10.009. PubMed PMID: 19879957.
7. Pazos E, Vazquez O, Mascarenas JL, Vazquez ME. Peptide-based fluorescent biosensors. Chemical Society reviews. 2009;38(12):3348-59. doi: 10.1039/b908546g. PubMed PMID: 20449054.

8. Blum AP, Kammeyer JK, Yin J, Crystal DT, Rush AM, Gilson MK, et al. Peptides Displayed as High Density Brush Polymers Resist Proteolysis and Retain Bioactivity. J Am Chem Soc. 2014;136(43):15422-37. doi: 10.1021/ja5088216.
9. Thompson MP, Randolph LM, James CR, Davalos AN, Hahn ME, Gianneschi NC. Labelling polymers and micellar nanoparticles via initiation, propagation and termination with ROMP. Polymer Chemistry. 2014;5(6):1954-64. doi: 10.1039/C3PY01338C.
10. Kammeyer JK, Blum AP, Adamiak L, Hahn ME, Gianneschi NC. Polymerization of protecting-group-free peptides via ROMP. Polymer Chemistry. 2013;4(14):3929-33. doi: 10.1039/C3PY00526G.
11. Patterson JP, Robin MP, Chassenieux C, Colombani O, O'Reilly RK. The analysis of solution self-assembled polymeric nanomaterials. Chemical Society Reviews. 2014;43(8):2412-25. doi: 10.1039/C3CS60454C.
12. Friedrich H, Frederik PM, de With G, Sommerdijk NAJM. Imaging of Self-Assembled Structures: Interpretation of TEM and Cryo-TEM Images. Angewandte Chemie International Edition. 2010;49(43):7850-8. doi: 10.1002/anie.201001493.
13. Cui H, Hodgdon TK, Kaler EW, Abezgauz L, Danino D, Lubovsky M, et al. Elucidating the assembled structure of amphiphiles in solution via cryogenic transmission electron microscopy. Soft Matter. 2007;3(8):945-55.
14. Talmon Y. Staining and Drying-Induced Artifacts in Electron Microscopy of Surfactant Dispersions. Journal of Colloid and Interface Science. 1983;93(2):366-82. doi: 10.1016/0021-9797(83)90420-4.
15. Ruska E. Beitrag zur übermikroskopischen Abbildung bei höheren Drucken. Kolloid-Zeitschrift. 1942;100(2):212-9. doi: 10.1007/BF01519549.
16. Abrams IM, McBain JW. A Closed Cell for Electron Microscopy. Journal of Applied Physics. 1944;15(8):607-9. doi: doi:http://dx.doi.org/10.1063/1.1707475.
17. Williamson MJ, Tromp RM, Vereecken PM, Hull R, Ross FM. Dynamic microscopy of nanoscale cluster growth at the solid-liquid interface. Nat Mater. 2003;2(8):532-6. doi: http://www.nature.com/nmat/journal/v2/n8/suppinfo/nmat944_S1.html.
18. Zhou H-C, Long JR, Yaghi OM. Introduction to Metal–Organic Frameworks. Chemical Reviews. 2012;112(2):673-4. doi: 10.1021/cr300014x.
19. Long JR, Yaghi OM. The pervasive chemistry of metal-organic frameworks. Chem Soc Rev. 2009;38(5):1213-4. doi: 10.1039/b903811f.
20. Kreno LE, Leong K, Farha OK, Allendorf M, Van Duyne RP, Hupp JT. Metal–Organic Framework Materials as Chemical Sensors. Chemical Reviews. 2011;112(2):1105-25. doi: 10.1021/cr200324t.
21. Lee J, Farha OK, Roberts J, Scheidt KA, Nguyen ST, Hupp JT. Metal-organic framework materials as catalysts. Chemical Society Reviews. 2009;38(5):1450-9. doi: 10.1039/B807080F.
22. Eddaoudi M, Kim J, Rosi N, Vodak D, Wachter J, O'Keeffe M, et al. Systematic design of pore size and functionality in isoreticular MOFs and their application in methane storage. Science (Washington, DC, U S). 2002;295(5554):469-72. doi: 10.1126/science.1067208.
23. Hoskins BF, Robson R. Infinite polymeric frameworks consisting of three dimensionally linked rod-like segments. Journal of the American Chemical Society. 1989;111(15):5962-4. doi: 10.1021/ja00197a079.
24. Cohen SM. Postsynthetic Methods for the Functionalization of Metal–Organic Frameworks. Chemical Reviews. 2011;112(2):970-1000. doi: 10.1021/cr200179u.
25. Murray LJ, Dinca M, Long JR. Hydrogen storage in metal-organic frameworks. Chemical Society Reviews. 2009;38(5):1294-314. doi: 10.1039/B802256A.

26. Li J-R, Sculley J, Zhou H-C. Metal–Organic Frameworks for Separations. Chemical Reviews. 2011;112(2):869-932. doi: 10.1021/cr200190s.
27. Fei H, Shin J, Meng YS, Adelhardt M, Sutter J, Meyer K, et al. Reusable Oxidation Catalysis Using Metal-Monocatecholato Species in a Robust Metal-Organic Framework. J Am Chem Soc. 2014;136(13):4965-73. doi: 10.1021/ja411627z.
28. Moh PY, Cubillas P, Anderson MW, Attfield MP. Revelation of the Molecular Assembly of the Nanoporous Metal Organic Framework ZIF-8. Journal of the American Chemical Society. 2011;133(34):13304-7. doi: 10.1021/ja205900f.
29. Moh PY, Brenda M, Anderson MW, Attfield MP. Crystallisation of solvothermally synthesised ZIF-8 investigated at the bulk, single crystal and surface level. CrystEngComm. 2013;15(45):9672-8. doi: 10.1039/C3CE40943K.
30. Shoaee M, Agger JR, Anderson MW, Attfield MP. Crystal form, defects and growth of the metal organic framework HKUST-1 revealed by atomic force microscopy. CrystEngComm. 2008;10(6):646-8. doi: 10.1039/B718890K.
31. Shoaee M, Anderson MW, Attfield MP. Crystal Growth of the Nanoporous Metal–Organic Framework HKUST-1 Revealed by In Situ Atomic Force Microscopy. Angewandte Chemie International Edition. 2008;47(44):8525-8. doi: 10.1002/anie.200803460.
32. de J, Niels, Ross FM. Electron microscopy of specimens in liquid. Nat Nanotechnol. 2011;6(11):695-704. doi: 10.1038/nnano.2011.161.
33. Zheng H, Smith RK, Jun Y-w, Kisielowski C, Dahmen U, Alivisatos AP. Observation of Single Colloidal Platinum Nanocrystal Growth Trajectories. Science. 2009;324(5932):1309-12.
34. Evans JE, Jungjohann KL, Browning ND, Arslan I. Controlled Growth of Nanoparticles from Solution with In Situ Liquid Transmission Electron Microscopy. Nano Lett. 2011;11(7):2809-13. doi: 10.1021/nl201166k.
35. Woehl TJ, Park C, Evans JE, Arslan I, Ristenpart WD, Browning ND. Direct observation of aggregative nanoparticle growth: kinetic modeling of the size distribution and growth rate. Nano Lett. 2014;14(1):373-8.
36. Woehl TJ, Evans JE, Arslan I, Ristenpart WD, Browning ND. Direct in Situ Determination of the Mechanisms Controlling Nanoparticle Nucleation and Growth. ACS Nano. 2012;6(10):8599-610. doi: 10.1021/nn303371y.
37. Liao H-G, Zherebetskyy D, Xin H, Czarnik C, Ercius P, Elmlund H, et al. Facet development during platinum nanocube growth. Science. 2014;345(6199):916-9.
38. Liao H-G, Zheng H. Liquid Cell Transmission Electron Microscopy Study of Platinum Iron Nanocrystal Growth and Shape Evolution. J Am Chem Soc. 2013;135(13):5038-43. doi: 10.1021/ja310612p.
39. Smeets PJM, Cho KR, Kempen RGE, Sommerdijk NAJM, De Yoreo JJ. Calcium carbonate nucleation driven by ion binding in a biomimetic matrix revealed by in situ electron microscopy. Nat Mater. 2015;advance online publication. doi: 10.1038/nmat4193

http://www.nature.com/nmat/journal/vaop/ncurrent/abs/nmat4193.html - supplementary-information.
40. Chen Q, Cho H, Manthiram K, Yoshida M, Ye X, Alivisatos AP. Interaction Potentials of Anisotropic Nanocrystals from the Trajectory Sampling of Particle Motion using in Situ Liquid Phase Transmission Electron Microscopy. ACS Central Science. 2015;1(1):33-9. doi: 10.1021/acscentsci.5b00001.
41. Chen X, Li C, Cao H. Recent developments of the in situ wet cell technology for transmission electron microscopies. Nanoscale. 2015;7(11):4811-9. doi: 10.1039/C4NR07209J.

42. Nielsen MH, Aloni S, De Yoreo JJ. In situ TEM imaging of CaCO3 nucleation reveals coexistence of direct and indirect pathways. Science. 2014;345(6201):1158-62.
43. d'Ischia M, Napolitano A, Ball V, Chen C-T, Buehler MJ. Polydopamine and Eumelanin: From Structure–Property Relationships to a Unified Tailoring Strategy. Accounts of Chemical Research. 2014;47(12):3541-50. doi: 10.1021/ar500273y.
44. Ju K-Y, Lee Y, Lee S, Park SB, Lee J-K. Bioinspired Polymerization of Dopamine to Generate Melanin-Like Nanoparticles Having an Excellent Free-Radical-Scavenging Property. Biomacromolecules. 2011;12(3):625-32. doi: 10.1021/bm101281b.
45. Liu Y, Ai K, Lu L. Polydopamine and Its Derivative Materials: Synthesis and Promising Applications in Energy, Environmental, and Biomedical Fields. Chemical Reviews. 2014;114(9):5057-115. doi: 10.1021/cr400407a.
46. Ai K, Liu Y, Ruan C, Lu L, Lu GM. Sp2 C-Dominant N-Doped Carbon Sub-micrometer Spheres with a Tunable Size: A Versatile Platform for Highly Efficient Oxygen-Reduction Catalysts. Advanced Materials. 2013;25(7):998-1003.
47. Ma S, Liu L, Bromberg V, Singler TJ. Electroless Copper Plating of Inkjet-Printed Polydopamine Nanoparticles: a Facile Method to Fabricate Highly Conductive Patterns at Near Room Temperature. ACS Appl Mater Interfaces. 2014;6(22):19494-8.
48. Ma S, Liu L, Bromberg V, Singler TJ. Fabrication of highly electrically conducting fine patterns via substrate-independent inkjet printing of mussel-inspired organic nano-material. Journal of Materials Chemistry C. 2014;2(20):3885-9.
49. Liu Y, Ai K, Liu J, Deng M, He Y, Lu L. Dopamine-Melanin Colloidal Nanospheres: An Efficient Near-Infrared Photothermal Therapeutic Agent for In Vivo Cancer Therapy. Advanced Materials. 2013;25(9):1353-9. doi: 10.1002/adma.201204683.
50. Stritzker J, Kirscher L, Scadeng M, Deliolanis NC, Morscher S, Symvoulidis P, et al. Vaccinia virus-mediated melanin production allows MR and optoacoustic deep tissue imaging and laser-induced thermotherapy of cancer. Proceedings of the National Academy of Sciences of the United States of America. 2013;110(9):3316-20.
51. Xiao M, Li Y, Allen MC, Deheyn DD, Yue X, Zhao J, et al. Bio-Inspired Structural Colors Produced via Self-Assembly of Synthetic Melanin Nanoparticles. ACS Nano. 2015;9(5):5454-60. doi: 10.1021/acsnano.5b01298.
52. Xiao M, Li Y, Zhao J, Wang Z, Gao M, Gianneschi NC, et al. Stimuli-Responsive Structurally Colored Films from Bioinspired Synthetic Melanin Nanoparticles. Chem Mater. 2016;28(15):5516-21.
53. Krogsgaard M, Behrens MA, Pedersen JS, Birkedal H. Self-Healing Mussel-Inspired Multi-pH-Responsive Hydrogels. Biomacromolecules. 2013;14(2):297-301. doi: 10.1021/bm301844u.
54. Li L, Smitthipong W, Zeng H. Mussel-inspired hydrogels for biomedical and environmental applications. Polymer Chemistry. 2015;6(3):353-8. doi: 10.1039/C4PY01415D.
55. Guo L, Liu Q, Li G, Shi J, Liu J, Wang T, et al. A mussel-inspired polydopamine coating as a versatile platform for the in situ synthesis of graphene-based nanocomposites. Nanoscale. 2012;4(19):5864-7. doi: 10.1039/c2nr31547e. PubMed PMID: 22945453.
56. Ju K-Y, Lee JW, Im GH, Lee S, Pyo J, Park SB, et al. Bio-Inspired, Melanin-Like Nanoparticles as a Highly Efficient Contrast Agent for T1-Weighted Magnetic Resonance Imaging. Biomacromolecules. 2013;14(10):3491-7. doi: 10.1021/bm4008138.
57. Miao Z-H, Wang H, Yang H, Li Z-L, Zhen L, Xu C-Y. Intrinsically Mn2+-Chelated Polydopamine Nanoparticles for Simultaneous Magnetic Resonance Imaging and Photothermal Ablation of Cancer Cells. ACS Applied Materials & Interfaces. 2015;7(31):16946-52. doi: 10.1021/acsami.5b06265.

58. Borg DC. TRANSIENT FREE RADICAL FORMS OF HORMONES: EPR SPECTRA FROM CATECHOLAMINES AND ADRENOCHROME. Proceedings of the National Academy of Sciences of the United States of America. 1965;53(3):633-9. PubMed PMID: PMC336989.
59. Sever MJ, Weisser JT, Monahan J, Srinivasan S, Wilker JJ. Metal-Mediated Cross-Linking in the Generation of a Marine-Mussel Adhesive. Angewandte Chemie International Edition. 2004;43(4):448-50. doi: 10.1002/anie.200352759.
60. Weisser JT, Nilges MJ, Sever MJ, Wilker JJ. EPR Investigation and Spectral Simulations of Iron−Catecholate Complexes and Iron−Peptide Models of Marine Adhesive Cross-Links. Inorganic Chemistry. 2006;45(19):7736-47. doi: 10.1021/ic060685p.
61. Burlamacchi L, Lai A, Monduzzi M, Saba G. NMR, EPR, and INDO Studies on the complexes of dopamine with Cu2+, Mn2+, and Fe3+ in aqueous solution. Journal of Magnetic Resonance (1969-1992). 1983;55(1):39-50. doi: http://dx.doi.org/10.1016/0022-2364(83)90275-5.
62. Lucarini M, Pedulli GF, Guerra M. A Critical Evaluation of the Factors Determining the Effect of Intramolecular Hydrogen Bonding on the O H Bond Dissociation Enthalpy of Catechol and of Flavonoid Antioxidants. Chemistry – A European Journal. 2004;10(4):933-9. doi: 10.1002/chem.200305311.
63. Bolzoni F, Giraudo S, Lopiano L, Bergamasco B, Fasano M, Crippa PR. Magnetic investigations of human mesencephalic neuromelanin. Biochim Biophys Acta, Mol Basis Dis. 2002;1586:210-8.
64. Aime S, Bergamasco B, Biglino D, Digilio G, Fasano M, Giamello E, et al. EPR investigations of the iron domain in neuromelanin. Biochim Biophys Acta, Mol Basis Dis. 1997;1361:49-58.
65. Gerlach M, Trautwein AX, Zecca L, Youdim MBH, Riederer P. Mossbauer spectroscopic studies of purified human neuromelanin isolated from the substantia nigra. J Neurochem. 1995;65:923-6.
66. Avdeef A, Sofen SR, Bregante TL, Raymond KN. Coordination chemistry of microbial iron transport compounds. 9. Stability constants for catechol models of enterobactin. J Am Chem Soc. 1978;100:5362-70.
67. Koenig SH, Brown 3rd RD, Spiller M, Chakrabarti B, Pande A. Intermolecular protein interactions in solutions of calf lens alpha-crystallin. Results from 1/T1 nuclear magnetic relaxation dispersion profiles. Biophysical Journal. 1992;61(3):776-85. doi: http://dx.doi.org/10.1016/S0006-3495(92)81882-9.
68. Aime S, Botta M, Terreno E. Gd(III)-BASED CONTRAST AGENTS FOR MRI. Advances in Inorganic Chemistry: Academic Press; 2005. p. 173-237.
69. Bertini I, C. Luchinat, and G. Parigi. Chapter 5 Transition metal ions: Shift and relaxation. In: Ivono Bertini CL, Giacomo P, editors. Current Methods in Inorganic Chemistry: Elsevier; 2001. p. 143-203.
70. Bertini I, Capozzi F, Luchinat C, Xia Z. Nuclear and electron relaxation of hexaaquairon(3+). The Journal of Physical Chemistry. 1993;97(6):1134-7. doi: 10.1021/j100108a006.
71. Bertini I, Galas O, Luchinat C, Messori L, Parigi G. A theoretical analysis of the 1H nuclear magnetic relaxation dispersion profiles of diferric transferrin. The Journal of Physical Chemistry. 1995;99(39):14217-22. doi: 10.1021/j100039a006.
72. Bertini I, Luchinat C, Nerinovski K, Parigi G, Cross M, Xiao Z, et al. Application of NMRD to Hydration of Rubredoxin and a Variant Containing a (Cys-S)3FeIII(OH) Site. Biophysical Journal. 2003;84(1):545-51. doi: http://dx.doi.org/10.1016/S0006-3495(03)74873-5.
73. Koenig SH, Brown 3rd RD, Lindstrom TR. Interactions of solvent with the heme region of methemoglobin and fluoro-methemoglobin. Biophysical Journal. 1981;34(3):397-408. doi: http://dx.doi.org/10.1016/S0006-3495(81)84858-8.

74. Li Y, Huang Y, Wang Z, Carniato F, Xie Y, Patterson JP, et al. Polycatechol Nanoparticle MRI Contrast Agents. Small. 2016;12(5):668-77. doi: 10.1002/smll.201502754.
75. Sitbon G, Bouccara S, Tasso M, Francois A, Bezdetnaya L, Marchal F, et al. Multimodal Mn-doped I-III-VI quantum dots for near infrared fluorescence and magnetic resonance imaging: from synthesis to in vivo application. Nanoscale. 2014;6(15):9264-72. doi: 10.1039/C4NR02239D.
76. Sarna T, Hyde JS, Swartz HM. Ion exchange in melanin: an electron spin resonance study with lanthanide probes. Science. 1976;192:1132-4.
77. Rabenstein MD, Shin Y-K. Determination of the distance between two spin labels attached to a macromolecule. Proc Natl Acad Sci U S A. 1995;92:8239-43.
78. Sebby KB, Walter ED, Usselman RJ, Cloninger MJ, Singel DJ. End-group distributions of multiple generations of spin-labeled PAMAM dendrimers. J Phys Chem B. 2011;115:4613-20.
79. Usselman RJ, Russek SE, Klem MT, Allen MA, Douglas T, Young M, et al. Temperature dependence of electron magnetic resonance spectra of iron oxide nanoparticles mineralized in Listeria innocua protein cages. J Appl Phys. 2012;112:084701.
80. Grillo VA, Hanson GR, Wang D, Hambley TW, Gahan LR, Murray KS, et al. Synthesis, X-ray Structural Determination, and Magnetic Susceptibility, Mössbauer, and EPR Studies of (Ph4P)2[Fe2(Cat)4(H2O)2]·6H2O, a Catecholato-Bridged Dimer of Iron(III). Inorganic Chemistry. 1996;35(12):3568-76. doi: 10.1021/ic950499b.
81. Anderson BF, Web J, Buckingham DA, Robertson GB. Crystal and molecular structure of piperidinium μ-acetato-di-μ-1,2-benzenediolato-bis-1,2-benzenediolatoferrate(III), (C5H12N)3 [(CH3COO){Fe(C6H4O2)2}2]: a compound of relevance to the 2Fe-active site of the respiratory protein hemerythrin. Bioinorganic Chemistry. 1982;16(1):21-32. doi: http://dx.doi.org/10.1016/S0162-0134(00)80242-1.
82. Ainscough EW, Brodie AM, McLachlan SJ, Brown KL. The reaction of 1,1[prime or minute]-biphenyl-2,2[prime or minute]-dial with iron(III) and the crystal structure of piperidinium bis[[small micro]-(1,1[prime or minute]-biphenyl-2,2[prime or minute]-diolato-O,[small micro]-O[prime or minute])(1,1[prime or minute]-biphenyl-2,2[prime or minute]-diolato-O,O[prime or minute])ferrate(III)]-ethanol(1/2). Journal of the Chemical Society Dalton Transactions. 1983(7):1385-9. doi: 10.1039/DT9830001385.
83. Fisher OZ, Larson BL, Hill PS, Graupner D, Nguyen-Kim M-T, Kehr NS, et al. Melanin-like Hydrogels Derived from Gallic Macromers. Advanced Materials. 2012;24(22):3032-6. doi: 10.1002/adma.201104437.
84. Felix CC, Hyde JS, Sarna T, Sealy RC. Interactions of melanin with metal ions. Electron spin resonance evidence for chelate complexes of metal ions with free radicals. Journal of the American Chemical Society. 1978;100(12):3922-6. doi: 10.1021/ja00480a044.
85. Gorun SM, Lippard SJ. Magnetostructural correlations in magnetically coupled (.mu.-oxo)diiron(III) complexes. Inorganic Chemistry. 1991;30(7):1625–30.
86. Taylor SW, Chase DB, Emptage MH, Nelson MJ, Waite JH. Ferric Ion Complexes of a DOPA-Containing Adhesive Protein from Mytilus edulis. Inorganic Chemistry. 1996;35(26):7572-7. doi: 10.1021/ic960514s.
87. Holten-Andersen N, Harrington MJ, Birkedal H, Lee BP, Messersmith PB, Lee KYC, et al. pH-induced metal-ligand cross-links inspired by mussel yield self-healing polymer networks with near-covalent elastic moduli. Proceedings of the National Academy of Sciences of the United States of America. 2011;108(7):2651-5.
88. Azuah RT, Kneller LR, Qiu Y. DAVE: A Comprehensive Software Suite for the Reduction, Visualization, and Analysis of Low Energy Neutron Spectroscopic Data. Journal of Research of the National Institute of Standards & Technology. 2009;114(6):341-58. PubMed PMID: 501513023.

(PECASE) Biomolecular Programming of Discrete Nanomaterials for Sensors, Templates and Mimics of

89. Sever MJ, Wilker JJ. Visible absorption spectra of metal-catecholate and metal-tironate complexes. Dalton Transactions. 2004(7):1061-72. doi: 10.1039/B315811J.
90. Prodi L, Rampazzo E, Rastrelli F, Speghini A, Zaccheroni N. Imaging agents based on lanthanide doped nanoparticles. Chemical Society Reviews. 2015;44(14):4922-52. doi: 10.1039/C4CS00394B.

AFOSR Deliverables Submission Survey

Response ID:7123 Data

1.

Report Type

Final Report

Primary Contact Email

Contact email if there is a problem with the report.

ngianneschi@ucsd.edu

Primary Contact Phone Number

Contact phone number if there is a problem with the report

8583737448

Organization / Institution name

UC San Diego

Grant/Contract Title

The full title of the funded effort.

Biomolecular Programming of Discrete Nanomaterials for Sensors, Templates and Mimics of Natural Nanoscale Assemblies

Grant/Contract Number

AFOSR assigned control number. It must begin with "FA9550" or "F49620" or "FA2386".

FA9550-11-1-0105

Principal Investigator Name

The full name of the principal investigator on the grant or contract.

Nathan C. Gianneschi

Program Officer

The AFOSR Program Officer currently assigned to the award

Hugh DeLong

Reporting Period Start Date

06/01/2011

Reporting Period End Date

08/31/2016

Abstract

We have worked on the development of biomolecule-polymer conjugates as responsive elements for assembly of complex morphology switchable nanomaterials, and have combined this with an effort in nature-inspired materials with a particular focus on synthetic, or artificial polymeric organelles, including melanosomes. Relevance of these projects to the DOD interests include the possibility of employing the resulting materials in advanced biochemical sensors, where recognition elements combined with stability and long term use are needed; hence our interest in stabilized but responsive biomolecular materials and conjugates between 2011 and 2016. In terms of melanin work, we see strong relevance in these bioinspired materials that are capable of acting as structural color elements, with unusually high refractive indices and with an understanding of synthetic processes leading to morphological control. This would lead to an ability to develop materials that have iridescent structural color, but capable of broad band absorbance, combined with unusual magnetic properties. The fact that very little is known about their natural biosynthesis, and their properties in general, means there is a rich source of chemical information to mine, and potentially utilize in new device applications. Thirdly, we have developed liquid cell TEM

(LCTEM) as a means for studying these complex responsive systems. This work has lead to our recent developments of instrumentation allowing the establishment of chemical gradients, and ongoing work to develop variable temperature LCTEM (VT-LCTEM) methodologies for looking at porous materials including covalent organic frameworks. The potential power of this technique is enormous. It would become the third arm in the TEM suite of characterization tools together with cryogenic, and standard high vacuum TEM. We anticipate that the kinds of tools described here for arraying and setting up the reactions is going to be a critical and commonplace tool. This is a tool that was patented, and we are currently pushing the technology to make it fit for inclusion in designs for dedicated liquid cell TEM instruments of the future. This would be the "Vitrobot" (an automated system for setting up cryogenic TEM experiments) of liquid cell TEM, and would allow anyone capable of performing standard TEM experiments to conduct what is now an extremely specialized and challenging imaging technique. Ongoing work will include methods for tracking particles automatically and quantifying their growth and motion in solution. This tool, implemented in real time, will allow the user to immediately assess the quality of the data, and to make decisions on the fly regarding how long to image and at what magnification. In summary, while there are many unsolved problems, they are all solvable, with a tremendous upside potential.

Distribution Statement

This is block 12 on the SF298 form.

Distribution A - Approved for Public Release

Explanation for Distribution Statement

If this is not approved for public release, please provide a short explanation. E.g., contains proprietary information.

SF298 Form

Please attach your SF298 form. A blank SF298 can be found here. Please do not password protect or secure the PDF The maximum file size for an SF298 is 50MB.

SF 298.pdf

Upload the Report Document. File must be a PDF. Please do not password protect or secure the PDF . The maximum file size for the Report Document is 50MB.

FINALReport_PECASE_2016_Compressed.pdf

Upload a Report Document, if any. The maximum file size for the Report Document is 50MB.

Archival Publications (published) during reporting period:

1) Chien, M. –P.; Thompson, M. P.; Gianneschi, N. C.; "DNA-nanoparticle micelles as supramolecular fluorogenic substrates enabling catalytic signal amplification and detection by DNAzyme probes" Chem. Comm., 2011, 47, 167-169

2) Ku, T.-H.; Chien, M.-P.; Thompson, M. P.; Sinkovits, R. S.; Olson, N. H; Baker, T. S.; Gianneschi, N. C. "Controlling and Switching the Morphology of Micellar Nanoparticles with Enzymes" J. Am. Chem. Soc. 2011, 133, 8392-8395

3) Chien, M. –P.; Gianneschi, N. C. "A Morphology Dependent Bioorganic Template for Inorganic Nanowire Synthesis" Small, 2011, 7, 2041-2046

4) Hahn, M. E.; Gianneschi, N. C. "Enzyme-Directed Assembly and Manipulation of Organic Nanomaterials." Chem. Comm., 2012, 47, 11814-11821

5) Randolph, L. M.; Chien, M. –P.; Gianneschi, N. C. "Biological Stimuli and Biomolecules in the Assembly and Manipulation of Nanoscale Polymeric Particles" Chem. Sci. 2012, 3, 1363-1380

6) Chien, M. –P.; Thompson, M. P.; Lin, E. C.; Gianneschi, N. C. "Fluorogenic Enzyme-Responsive Micellar Nanoparticles" Chem. Sci. 2012, 3, 2690-2694

7) Chien, M.-P.; Carlini, A. S.; Hu, D.; Barback, C. V.; Rush, A. M.; Hall, D. J.; Orr, G.; Gianneschi, N. C. "Enzyme-Directed Assembly of Nanoparticles in Tumors Monitored by In Vivo Whole Animal and Ex Vivo Super Resolution Fluorescence Imaging" J. Am. Chem. Soc. 2013, 135, 18710-18713

8) Chien, M. –P.; Thompson, M. P.; Barback, C. V.; Hall, D. J.; Gianneschi, N. C. "Enzyme-Directed Assembly of a Nanoparticle Probe in Tumor Tissue" Advanced Materials. 2013, 25, 3599-3604.

9) Kammeyer, J. K.; Blum, A. P.; Adamiak, L. Hahn, M. E.; Gianneschi, N. C. "Polymerization of Protecting-Group-Free Peptides via ROMP" Polymer Chemistry 2013, 4, 3929-3933

10) Rush, A. M.; Thompson, M. P.; Tatro, E. T.; Gianneschi, N. C. "Nuclease-resistant DNA via High Density Packing in Polymeric Micellar Nanoparticle Coronas" ACS Nano 2013, 7, 1379-1387
11) Hahn, M. E.; Randolph, L. M.; Adamiak, L.; Thompson, M. P.; Gianneschi, N. C. "Polymerization of a Peptide-Based Enzyme Substrate" Chem. Commun. 2013, 49, 2873-2875
12) Proetto, M. T.; Rush, A. M.; Chien, M. –P.; Abellan Baeza, P.; Patterson, J. P.; Thompson, M. P.; Olson, N. H.; Moore, C. E.; Rehingold, A. L.; Andolina, C.; Millston, J.; Howell, S. B.; Browning, N D.; Evans, J. E..; Gianneschi, N. C. "Dynamics of Soft Materials Captured by Transmission Electron Microscopy" J. Am. Chem. Soc. 2014, 136, 1162-1165.
13) Thompson, M. P.; Randolph, L. M.; James, C. R.; Davalos, A. N.; Hahn, M. E. Gianneschi, N. C. "Labeling Polymers and Micellar Nanoparticles via Initiation, Propagation and Termination with ROMP" Polymer Chemistry 2014, 5, 1954-1964
14) Rush, A. M.; Nelles, D. A.; Blum, A. P.; Barnhill, S. A.; Tatro, E. T.; Yeo, G. W.; Gianneschi, N. C. "Intracellular mRNA Regulation with Self-Assembled Locked Nucleic Acid Polymer Nanoparticles" J. Am. Chem. Soc. 2014, 136, 7615-7618.
15) James, C. R.; Rush, A. M.; Insley, T.; Vukovic, L.; Kral, P.; Gianneschi, N. C. "Poly(oligonucleotide)" J. Am. Chem. Soc. 2014, 136, 11216-11219.
16) Blum, A. P.; Kammeyer, J. K.; Yin, J.; Crystal, D. T.; Rush, A. M.; Gilson, M. K. Gianneschi, N. C. "Peptides Displayed as High Density Brush Polymers Resist Proteolysis and Retain Bioactivity" J Am. Chem. Soc. 2014, 136, 15422-15437
17) Ku, T.-H.; Sahu, S.; Kosa, N.; Pham, K. M.; Burkart, M. D.; Gianneschi, N. C. Tapping a Bacterial Enzymatic Pathway for the Preparation and Manipulation of Synthetic Nanomaterials. J. Am. Chem. Soc. 2014, 136, 17378-17381
18) Blum, A.P.; Kammeyer, J.K.; Rush, A.M.; Callmann, C.E.; Hahn, M.E.; Gianneschi N. C. Stimuli-Responsive Nanomaterials for Biomedical Applications. J. Am. Chem. Soc. 2014, 137, 2140-2154
19) Bell, N. C.; Doyle, S. J; Battistelli, G.; LeGuyader, C. L. M.; Thompson, M. P.; Poe, A. M; Rheingold, A.; Moore, C.; Montalti, M.; Thayumanavan, S.; Tauber, M. J; Gianneschi, N. C. "Dye Encapsulation in Polynorbornene Micelles" Langmuir 2015, 31, 9707-9717.
20) Barnhill, S. A.; Bell, N. C.; Patterson, J. P.; Olds, D. P.; Gianneschi, N. C. Phase Diagrams of Polynorbornene Amphiphilic Block Copolymers in Solution. Macromolecules 2015, 48, 1152-1161
21) Xiao, M.; Li, Y.; Allen, M.; Deheyn, D.; Yue, X.; Zhao, J.; Gianneschi, N. C. Shawkey, M.; Dhinojwala, A. Bioinspired Structural Colors Produced via Self-Assembly of Synthetic Melanin Nanoparticles. ACS Nano, 2015, 9, 5454-5460.
22) Patterson, J. P.; Abellan, P.; Denny, M. S.; Park, C.; Browning, N. D.; Cohen, S. M.; Evans, J. E.; Gianneschi, N. C. "Observing the Growth of Metal-Organic Frameworks by In Situ Liquid Cell TEM" J. Am. Chem. Soc. 2015, 137, 7322-7328.
23) Ma, C. D.; Adamiak, L.; Miller, D. S.; Wang, X.; Gianneschi, N. C.; Abbott, N. L. "Liquid Crystal Interfaces Programmed with Enzyme-Responsive Polymers and Surfactants" Small 2015, 11, 5747-5751.
24) Blum, A. P.; Kammeyer, J. K.; Gianneschi, N. C. "Activating Peptides for Cellular Uptake via Polymerization into High Density Brushes" Chemical Science 2016, 7, 989-994.
25) Patterson, J. P.; Parent, L. R.; Cantlon, J.; Eickhoff, H.; Bared, G.; Evans, J. E.; Gianneschi, N. C. "Picoliter Drop-On-Demand Dispensing for Multiplex Liquid Cell TEM" Microscopy and Microanalysis 2016, 22, 507-514.
26) Carlini, A. S.; Adamiak, L.; Gianneschi, N. C. "Biosynthetic Polymers as Functional Materials" Macromolecules 2016, 49, 4379-4394.
27) Xiao, M.; Li, Y.; Zhao, J.; Wang, Z.; Gao, M.; Gianneschi, N. C.; Dhinojwala, A.; Shawkey, M. D. "Stimuli-Responsive Structurally Colored Films from Bioinspired Synthetic Melanin Nanoparticles" Chemistry of Materials 2016, 28, 5516-5521

New discoveries, inventions, or patent disclosures:

Do you have any discoveries, inventions, or patent disclosures to report for this period?

Yes

Please describe and include any notable dates

2012-207: New Methods for Arranging and Packaging Nucleic Acids for Unusual Resistance to Nucleases

and Targeted Delivery for Gene Therapy
http://techtransfer.universityofcalifornia.edu/NCD/23489.html

2015-015: Polymerizing Nucleic Acids
http://techtransfer.universityofcalifornia.edu/NCD/24367.html

2015-036: Displaying Peptides as High Density Brush Polymers Ensures Bioactivity, Proteolytic Resistance, and Cellular Uptake
http://techtransfer.universityofcalifornia.edu/NCD/24556.html

2016-328: Polydopamine-based artificial melanins as intracellular UV-shield
2016-026: Low volume drop dispensing liquid cell electron microscopy sample preparation

Do you plan to pursue a claim for personal or organizational intellectual property?

Yes

Changes in research objectives (if any):

Change in AFOSR Program Officer, if any:

Extensions granted or milestones slipped, if any:

AFOSR LRIR Number

LRIR Title

Reporting Period

Laboratory Task Manager

Program Officer

Research Objectives

Technical Summary

Funding Summary by Cost Category (by FY, $K)

	Starting FY	FY+1	FY+2
Salary			
Equipment/Facilities			
Supplies			
Total			

Report Document

Report Document - Text Analysis

Report Document - Text Analysis

Appendix Documents

2. Thank You

E-mail user

Oct 15, 2016 21:10:38 Success: Email Sent to: ngianneschi@ucsd.edu